development of neuropathic pain after spinal nerve injury remains to be established.

CCL21 as potential drug target to prevent neuropathic pain

Whether or not blocking of CCL21 would be of therapeutic relevance to stop already ongoing neuropathic pain is unknown. Since CCL21 expression peaked very early after nerve injury and diminished thereafter and since the stop of CCL21-blocking antibody treatment did not lead to increased pain states for >10 subsequent days, our data might not argue for a role of CCL21 in the maintenance of neuropathic pain. The data presented in this study strongly indicate that inhibition of CCL21 expression in DRG neurons or attenuation of its function in the dorsal horn would prevent the development of neuropathic pain, which would be a welcomed therapeutic intervention for patients with acute nerve injury. Anatomical considerations might support the possibility that similar processes are also occurring in humans. In rodents it is known that microglia activity and subsequent development of neuropathic pain depends on an intact dorsal root, indicating the transport of activating molecules (Colburn *et al*, 1999; Obata *et al*, 2006a, b). In humans cutting of dorsal roots (e.g. to treat spasticity or for tumour removal) does not lead to neuropathic pain, in contrast to lesions distal from the DRG (Campbell and Meyer, 2006), which might suggest a transport of microglia-activating molecules through the dorsal root also in humans. Whether or not CCL21 is also expressed in human DRG neurons in response to nerve injury, however, remains to be established.

Taken together, we provide evidence that neuronal CCL21 in mice is a rapid signal that up-regulates P2X4 receptor expression in spinal cord microglia, identifying CCL21 as the neuronal signal that is required and sufficient for the induction of tactile allodynia after spinal nerve injury.

Materials and methods

Animals

plt (Mori *et al*, 2001; Nakano and Gunn, 2001) and wild-type C57BL/6 mice (Clea Japan) were used. Animals were housed in groups of two to three per cage at a temperature of 22±1 °C with a 12-h light–dark cycle (light on from 08:30 to 20:30 hours), and fed food and water *ad libitum*. All animal experiments were conducted according to relevant national and international guidelines 'Act on Welfare and Management of Animals' (Ministry of Environment of Japan) and 'Regulation of Laboratory Animals' (Kyushu University), and under the protocols approved by the Institutional Animal Care and Use committee review panels at Kyushu University.

Spinal nerve injury

We used the spinal nerve injury model (Kim and Chung, 1992) with some modifications (Tozaki-Saitoh *et al*, 2008; Tsuda *et al*, 2009b) in 9- to 12-week-old mice. Under isoflurane (2%) anaesthesia, a small left-side incision at ~L4–S2 was made. Paraspinal muscle and fat were removed from the L6 traverse process, and the part of this traverse process was removed to expose the parallel-lying L4 and L5 spinal nerves. The L5 nerve was isolated and cut. The wound was sutured with 3-0 silk. The surrounding skin was pulled together and sutured with 3-0 silk.

Behavioural studies

To assess the tactile allodynia, mice were placed individually in an opaque plastic cylinder, which was placed on a wire mesh and habituated for 1 h to allow acclimatization to the new environment. After that, calibrated von Frey filaments (0.02–2.0 g, Stoelting) were applied to the plantar surface of the hindpaw from below the mesh floor, and the 50% PWT was determined using the up–down method (Chaplan *et al*, 1994). The PWT was measured before and after the injury of the L5 spinal nerve (an animal model of neuropathic pain) or intrathecal administration of recombinant CCL21 (0.06 μg/mouse, R&D Systems). Intrathecal administration to mice was performed according to a procedure described previously (Tsuda *et al*, 2008a) using a 25-μl Hamilton syringe with 30-gauge needle. A neutralizing antibody for CCL21 (0.3 μg/mouse, Peprotech) was administered intrathecally twice a day from day 0 (15 min before nerve injury) to day 3. Nerve injury-induced thermal hyperalgesia was assessed using hot-plate test. Mice were placed on a metal surface maintained at either 49 °C within a 25-cm-high Plexiglas box (25 cm^2). The latency to either lick or shake the hindpaw was measured as a nocifensive end point. Noxious heat-evoked hindpaw withdrawal responses were detected by the application of radiant heat (Ugo Basile, Italy) to the tail and the plantar surface of hindpaw, respectively (Tsuda *et al*, 2007). The intensity of the heat stimulus was adjusted to 30 or 50 V, and the latency of the paw withdrawal response (seconds) was measured (Tsuda *et al*, 2007). The sensitivity to noxious mechanical stimulus was assessed by measuring the frequency of withdrawal responses to application of a von Frey filament (2.0 g) 10 times. Motor coordination was assessed using the rotarod performance test (Tsuda *et al*, 2007).

Immunohistochemistry

According to a procedure described previously (Nakajima *et al*, 1992), anaesthetized mice were perfused transcardially with PBS, followed by 4% paraformaldehyde. The fifth lumbar (L5) segments of the DRG, dorsal root and spinal cord were removed, post-fixed in the same fixative for 3 h at 4 °C, and placed in 30% sucrose solution for 24 h at 4 °C. Sections (30 μm) were cut and processed for immunohistochemistry with antibodies for CCL21 (1:500, Peprotech), TRPV1 (1:1000, Santa Cruz), isolectin B4 (1:200, Sigma), CGRP (1:20 000, Peninsula Laboratories), NF200 (1:400, Sigma), OX-42 (1:1000, Serotec), Iba1 (1:2000, Wako), Lyn (1:200, Wako), phosphorylated-histone H3 (Ser10) (p-HisH3, 1:1000, Upstate/Millipore), CD3 (1:100, eBioscience) and P2X4 (1:1000, kindly provided by Dr Francois Rassendren) (Ulmann *et al*, 2008). Following incubation, the sections were incubated with secondary antibodies conjugated to Alexa Fluor™ 488 or 546 (1:1000, Molecular Probes). The sections were analysed using an LSM510 Imaging System (Zeiss). For the cell size-frequency analyses, the cross-sectional areas of total and CCL21-positive DRG neurons with clearly visible nuclei were measured.

Microglial culture

Primary cultured microglia were prepared in accordance with a method described previously (Nakajima *et al*, 1992). In brief, a mixed glial culture was prepared from neonatal Wistar rats, C57BL/6 and *plt* mice and maintained for 10–16 days in DMEM with 10% fetal bovine serum. Immediately before experiments, microglia were collected by a gentle shake as the floating cells over the mixed glial culture. The microglia were transferred to coverslips for subsequent experiments. The cultures were of >99% purity, determining by immunostaining for OX-42 and Iba1.

Western blotting

Whole-cell lysates of cultured microglial cells were prepared in accordance with the methods described previously (Tsuda *et al*, 2008b). Aliquots (4 μg) were subjected to a 10% polyacrylamide gel electrophoresis (Bio-Rad), and proteins were transferred electrophoretically to nitrocellulose membranes. After blocking, the membranes were incubated with anti-$P2X_4R$ rabbit polyclonal antibody (1:1000, Alomone) or anti-β-actin (1:2000, Sigma) then incubated with HRP-conjugated secondary antibody (1:1000). The blots were detected using ECL western blotting detection system (GE Healthcare) and an LAS-3000 imaging system (Fujifilm). Bands were quantified using the software NIH Image J 1.36.

Real-time PCR

Real-time amplification, using an iCycler (Bio-Rad) and iQ SYBR Green supermix (Bio-Rad), was performed on 4 ng cDNA derived from microglia culture or spinal cord tissue. RNA preparation and cDNA synthesis was performed as described

recently (Dijkstra *et al*, 2006). The primers used for real-time PCR were designed using Primer Designer (Scientific and Educational Software, Version 3.0) and have been published earlier (Dijkstra *et al*, 2006). PCR amplification with CCR7 and CXCR3 primers was run in parallel with primers for the housekeeping gene hydroxymethylbilane synthase and quantified as described recently (Dijkstra *et al*, 2006). Primers used for P2X4 were (F): 5′-TGG CGGACTATGTGATTCCA-3′, primer (B): 5′-GGTTCACGGTGACGATC ATG-3′. Lymph node tissue served as positive control and reference for CCR7 and CXCR3 expression.

Statistics

Statistical analyses of the results were made with Student's *t*-test, Mann–Whitney *U*-test or two-way repeated measures ANOVA (*post hoc* test using Tukey).

Supplementary data

Supplementary data are available at *The EMBO Journal* Online (http://www.embojournal.org).

Acknowledgements

This work was supported by Dutch NWO-Vidi grant, Deutsche Forschungsgemeinschaft (DFG, FOR 1336) and a stipend from Kyushu University (KB), and by grants from the Ministry of Education, Culture, Sports, Science and Technology of Japan (MT, HT-S, KI) and in part from the Mochida Memorial Foundation for Medical and Pharmaceutical Research and the Astellas Foundation for Research on Metabolic Disorders (MT). We thank Drs Terutaka Kakiuchi, Fumio Ishikawa and Taku Kuwabara (Toho University School of Medicine, Tokyo, Japan) for providing some *plt* mice. We also thank Dr Francois Rassendren (Institut de Génomique Fonctionnelle, Montpellier, France) for providing the antibody for P2X4. KB, MT, HS-T, KT, TM and ET performed the experimental work. KB, MT and KI planned the project and designed the experiments. KB, MT, HB and KI wrote the manuscript.

Conflict of interest

The authors declare that they have no conflict of interest.

References

Abbadie C (2005) Chemokines, chemokine receptors and pain. *Trends Immunol* **26:** 529–534

Biber K, Neumann H, Inoue K, Boddeke HWGM (2007) Neuronal on and off signals control microglia. *Trends Neurosci* **30:** 598–602

Biber K, Sauter A, Brouwer N, Copray SCVM, Boddeke HWGM (2001) Ischemia-induced neuronal expression of the microglia attracting chemokine secondary lymphoid-tissue chemokine (SLC). *Glia* **34:** 121–133

Biber K, Vinet J, Boddeke HWGM (2008) Neuron-microglia signaling: chemokines as versatile messengers. *J Neuroimmunol* **198:** 69–74

Campbell JN, Meyer RA (2006) Mechanisms of neuropathic pain. *Neuron* **52:** 77–92

Cardona AE, Pioro EP, Sasse ME, Kostenko V, Cardona SM, Dijkstra IM, Huang D, Kidd G, Dombrowski S, Dutta R, Lee JC, Cook DN, Jung S, Lira SA, Littman DR, Ransohoff RM (2006) Control of microglial neurotoxicity by the fractalkine receptor. *Nat Neurosci* **9:** 917–924

Chaplan SR, Bach FW, Pogrel JW, Chung JM, Yaksh TL (1994) Quantitative assessment of tactile allodynia in the rat paw. *J Neurosci Methods* **53:** 55–63

Colburn RW, Rickman AJ, DeLeo JA (1999) The effect of site and type of nerve injury on spinal glial activation and neuropathic pain behavior. *Exp Neurol* **157:** 289–304

Coull JA, Beggs S, Boudreau D, Boivin D, Tsuda M, Inoue K, Gravel C, Salter MW, De Koninck Y (2005) BDNF from microglia causes the shift in neuronal anion gradient underlying neuropathic pain. *Nature* **438:** 1017–1021

Coyle DE (1998) Partial peripheral nerve injury leads to activation of astroglia and microglia which parallels the development of allodynic behavior. *Glia* **23:** 75–83

Davalos D, Grutzendler J, Yang G, Kim JV, Zuo Y, Jung S, Littman DR, Dustin ML, Gan WB (2005) ATP mediates rapid microglial response to local brain injury *in vivo*. *Nat Neurosci* **8:** 752–758

de Jong EK, Dijkstra IM, Hensens M, Brouwer N, Amerongen M, Liem RSB, Boddeke HWMG, Biber K (2005) Vesicle-mediated transport and release of CCL21 in endangered neurons: a possible explanation for microglia activation remote from a primary lesion. *J Neurosci* **25:** 7548–7557

de Jong EK, Vinet J, Stanulovic V, Wesseling EM, Meijer M, Schollema K, Boddeke HWGM, Biber K (2008) Expression, transport and axonal sorting of neuronal CCL21 in large dense core vesicles. *FASEB J* **22:** 4136–4145

Dijkstra IM, De Haas A, Brouwer N, Boddeke HWGM, Biber K (2006) Challenge with innate and protein antigens induces CCR7 expression by microglia *in vitro* and *in vivo*. *Glia* **54:** 861–872

Guseva D, Chelyshev Y (2006) The plasticity of the DRG neurons belonging to different subpopulations after dorsal rhizotomy. *Cell Mol Neurobiol* **26:** 1226–1234

Hains BC, Waxman SG (2006) Activated microglia contribute to the maintenance of chronic pain after spinal cord injury. *J Neurosci* **26:** 4308–4317

Hanisch UK, Kettenmann H (2007) Microglia: active sensor and versatile effector cells in the normal and pathological brain. *Nat Neurosci* **10:** 1387–1394

Haynes SE, Hollopeter G, Yang G, Kurpius D, Dailey ME, Gan WB, Julius D (2006) The P2Y12 receptor regulates microglial activation by extracellular nucleotides. *Nat Neurosci* **9:** 1512–1519

Kim SH, Chung JM (1992) An experimental model for peripheral neuropathy produced by segmental spinal nerve ligation in the rat. *Pain* **50:** 355–363

Koizumi S, Shigemoto-Mogami Y, Nasu-Tada K, Shinozaki Y, Ohsawa K, Tsuda M, Joshi BV, Jacobson KA, Kohsaka S, Inoue K (2007) UDP acting at P2Y6 receptors is a mediator of microglial phagocytosis. *Nature* **446:** 1091–1095

Lashbrook JM, Ossipov MH, Hunter JC, Raffa RB, Tallarida RJ, Porreca F (1999) Synergistic antiallodynic effects of spinal morphine with ketorolac and selective COX1- and COX2-inhibitors in nerve-injured rats. *Pain* **82:** 65–72

Miller RJ, Rostene W, Apartis E, Banisadr G, Biber K, Milligan ED, White FA, Zhang J (2008) Chemokine action in the nervous system. *J Neurosci* **28:** 11792–11795

Mori S, Nakano H, Aritomi K, Wang CR, Gunn MD, Kakiuchi T (2001) Mice lacking expression of the chemokines CCL21-ser and CCL19 (plt mice) demonstrate delayed but enhanced T cell immune responses. *J Exp Med* **193:** 207–218

Nakajima K, Shimojo M, Hamanoue M, Ishiura S, Sugita H, Kohsaka S (1992) Identification of elastase as a secretory protease from cultured rat microglia. *J Neurochem* **58:** 1401–1408

Nakano H, Gunn MD (2001) Gene duplications at the chemokine locus on the mouse chromosome 4: multiple strain-specific haplitypes and the deletion of secondary lymphpoid-organ chemokine and EBI-1 ligand chemokine genes in the *plt* mutation. *J Immunol* **166:** 361–369

Obata K, Katsura H, Sakurai J, Kobayashi K, Yamanaka H, Dai Y, Fukuoka T, Noguchi K (2006a) Suppression of the p75 neurotrophin receptor in uninjured sensory neurons reduces neuropathic pain after nerve injury. *J Neurosci* **26:** 11974–11986

Obata K, Yamanaka H, Kobayashi K, Dai Y, Mizushima T, Katsura H, Fukuoka T, Tokunaga A, Noguchi K (2006b) The effect of site and type of nerve injury on the expression of brain-derived neurotrophic factor in the dorsal root ganglion and on neuropathic pain behavior. *Neuroscience* **137:** 961–970

Raghavendra V, Tanga F, DeLeo JA (2003) Inhibition of microglial activation attenuates the development but not existing hypersensitivity in a rat model of neuropathy. *J Pharmacol Exp Ther* **306:** 624–630

Ransohoff RM, Perry VH (2009) Microglial physiology: unique stimuli, specialized responses. *Annu Rev Immunol* **27:** 119–145

Rappert A, Bechmann I, Pivneva T, Mahlo J, Biber K, Nolte C, Kovac A, Gerard C, Boddeke HWGM, Nitsch R, Kettenmann H (2004) CXCR3-dependent microglial recruitment is essential for dendritic loss after brain lesion. *J Neurosci* **24:** 8500–8509

Rappert A, Biber K, Nolte C, Lipp M, Schubel A, Lu B, Gerard NP, Gerard C, Boddeke HWMG, Kettenmann H (2002) Secondary lymphoid tissue chemokine (CCL21) activates CXCR3 to trigger a Cl^- current and chemotaxis in murine microglia. *J Immunol* **169:** 3221–3226

Saab CY, Haines BC (2009) Remote neuroimmune signaling: a long-range mechanism of nociceptive network plasticity. *Trends Neurosci* **32:** 110–117

Scholz J, Woolf CJ (2007) The neuropathic pain triad: neurons, immune cells and glia. *Nat Neurosci* **10:** 1361–1368

Tozaki-Saitoh H, Tsuda M, Miyata H, Ueda K, Kohsaka S, Inoue K (2008) P2Y12 receptors in spinal microglia are required for neuropathic pain after peripheral nerve injury. *J Neurosci* **28:** 4949–4956

Tsuda M, Inoue K, Salter MW (2005) Neuropathic pain and spinal microglia: a big problem from molecules in "small" glia. *Trends Neurosci* **28:** 101–107

Tsuda M, Ishii S, Masuda T, Hasegawa S, Nakamura K, Nagata K, Yamashita T, Furue H, Tozaki-Saitoh H, Yoshimura M, Koizumi S, Shimizu T, Inoue K (2007) Reduced pain behaviors and extracellular signal-related protein kinase activation in primary sensory neurons by peripheral tissue injury in mice lacking platelet-activating factor receptor. *J Neurochem* **102:** 1658–1668

Tsuda M, Kohro Y, Yano T, Tsujikawa T, Kitano J, Tozaki-Saitoh H, Koyanagi S, Ohdo S, Ji RR, Salter MW, Inoue K (2011) JAK-STAT3 pathway regulates spinal astrocyte proliferation and neuropathic pain maintenance in rats. *Brain*, In press

Tsuda M, Kuboyama K, Inoue T, Nagata K, Tozaki-Saitoh H, Inoue K (2009a) Behavioral phenotypes of mice lacking purinergic P2X4 receptors in acute and chronic pain assays. *Mol Pain* **5:** 28

Tsuda M, Masuda T, Kitano J, Shimoyama H, Tozaki-Saitoh H, Inoue K (2009b) IFN-gamma receptor signaling mediates spinal microglia activation driving neuropathic pain. *Proc Natl Acad Sci USA* **106:** 8032–8037

Tsuda M, Shigemoto-Mogami Y, Koizumi S, Mizokoshi A, Kohsaka S, Salter MW, Inoue K (2003) P2X4 receptors induced in spinal microglia gate tactile allodynia after nerve injury. *Nature* **424:** 778–783

Tsuda M, Toyomitsu E, Komatsu T, Masuda T, Kunifusa E, Nasu-Tada K, Koizumi S, Yamamoto K, Ando J, Inoue K (2008a) Fibronectin/integrin system is involved in P2X(4) receptor upregulation in the spinal cord and neuropathic pain after nerve injury. *Glia* **56:** 579–585

Tsuda M, Tozaki-Saitoh H, Masuda T, Toyomitsu E, Tezuka T, Yamamoto T, Inoue K (2008b) Lyn tyrosine kinase is required for P2X(4) receptor upregulation and neuropathic pain after peripheral nerve injury. *Glia* **56:** 50–58

Ulmann L, Hatcher JP, Hughes JP, Chaumont S, Green PJ, Conquet F, Buell GN, Reeve AJ, Chessell IP, Rassendren F (2008) Up-regulation of P2X4 receptors in spinal microglia after peripheral nerve injury mediates BDNF release and neuropathic pain. *J Neurosci* **28:** 11263–11268

Watkins LR, Milligan ED, Maier SF (2001) Glia cells: a driving force for pathological pain. *Trends Neurosci* **24:** 450–455

Wegert S, Ossipov MH, Nichols ML, Bian D, Vanderah TW, Malan Jr TP, Porreca F (1997) Differential activities of intrathecal MK-801 or morphine to alter responses to thermal and mechanical stimuli in normal or nerve-injured rats. *Pain* **71:** 57–64

White FA, Jung H, Miller RJ (2007) Chemokines and the pathophysiology of neuropathic pain. *Proc Natl Acad Sci* **104:** 20151–20158

Van Weering HR, Jong AP, Haas AH, Biber K, Boddeke HW (2010) CCL21-induced calcium transients and proliferation in primary mouse astrocytes: CXCR3-dependent and independent responses. *Brain Behav Immun* **24:** 768–775

PAIN® 153 (2012) 68–79

PAIN®

www.elsevier.com/locate/pain

Re-evaluation of the phenotypic changes in L4 dorsal root ganglion neurons after L5 spinal nerve ligation

Tetsuo Fukuoka [a,b,*], Hiroki Yamanaka [a], Kimiko Kobayashi [a], Masamichi Okubo [a], Kan Miyoshi [a], Yi Dai [c], Koichi Noguchi [a]

[a] Department of Anatomy and Neuroscience, Hyogo College of Medicine, Nishinomiya, Hyogo, Japan
[b] Pain Mechanism Research Group, Hyogo College of Medicine, Nishinomiya, Hyogo, Japan
[c] Department of Pharmacy, School of Pharmacy, Hyogo University of Health Sciences, Kobe, Japan

Sponsorships or competing interests that may be relevant to content are disclosed at the end of this article.

ARTICLE INFO

Article history:
Received 5 March 2011
Received in revised form 29 August 2011
Accepted 12 September 2011

Keywords:
Neuropathic pain model
Spared neuron
Sodium channel
Brain-derived neurotrophic factor

ABSTRACT

The L5 spinal nerve ligation (SNL) is a widely used animal neuropathic pain model. There are conflicting reports regarding the extent of injury to the L4 dorsal root ganglion (DRG) neurons in this model. If a significant number of these neurons were injured, the previously reported phenotypic and electrophysiological changes at this level are in need of re-evaluation by separating the injured neurons and the frankly spared ones. So, we immunostained activating transcription factor 3 (ATF3) and examined the change in expression of transcripts for neuropeptide Y (NPY), brain-derived neurotrophic factor (BDNF) and several voltage-gated sodium channel α-subunits (Nav1.1, Nav1.3, Nav1.6, Nav1.7, Nav1.8, and Nav1.9) in the L4 DRG by comparing signal intensities of individual neurons using *in situ* hybridization histochemistry. ATF3-immunoreactivity was similarly observed in 4–6% of neuronal nuclei of the SNL and sham-operated ipsilateral L4 DRGs. Comparison between ATF3+ and ATF3− neurons in the SNL L4 DRG revealed that (1) whereas NPY induction occurred in ATF3+ cells, BDNF increased mainly in ATF3− neurons; (2) although ATF3+ neurons had higher Nav1.3 signals than ATF3− neurons, these signals were much lower than those of the L5 DRG neurons; and (3) ATF3+/N52− neurons selectively lost Nav1.8 and Nav1.9 mRNAs. Comparison of the total neuronal populations among naïve, SNL, and sham-operated rats revealed no significant differences for all examined Nav mRNAs. Because neuropathic pain behaviors were developed by rats with SNL but not the sham-operation, the small number of injured L4 neurons likely do not contribute to the pathomechanisms of neuropathic pain.

1. Introduction

Widely used animal neuropathic pain models include partial nerve injury of the sciatic nerve components [15]. Among them, the L5 spinal nerve ligation (SNL) model is unique in that the directly injured L5 dorsal root ganglion (DRG) neurons and the potentially spared L4 DRG neurons are anatomically separated [23]. There is compelling evidence indicating that the L4 primary afferents change the expression of some pain-related molecules and that these changes have important roles in pathomechanisms for abnormal pain behavior in this model. For example, mRNAs for preprotachykinin (PPT), calcitonin-gene related peptide (CGRP), TRPV1, TRPA1, and brain-derived neurotrophic factor (BDNF) increase in the L4 DRG neurons following L5 SNL [13,16,17,19,20,22,34]. Indeed, early studies have demonstrated that several axonal injury-induced phenotypic changes occur in the L5 but not in the L4 DRG in this model, including the up-regulation of neuropeptide Y (NPY), galanin, vasoactive intestinal peptide, c-jun, and activating transcription factor 3 (ATF3) [8,16,34,35,44]. More recent reports, however, have found that 11–40% of L4 DRG neurons contain ATF3-positive (+) nuclei, suggesting that some L4 DRG neurons are injured [10,40]. Because PPT, CGRP, and BDNF mRNAs increase also in the directly injured neurons [6,29,30,32], these two reports cast doubt whether these molecules are up-regulated by the frankly spared L4 DRG neurons.

This is also the case for the spontaneous discharge of the injured primary afferents. Such abnormal activity is thought to be responsible for triggering and maintaining neuropathic pain behavior by increasing the excitability of spinal dorsal horn neurons [9]. Although multiple ion channels are involved in neuronal electro-

* Corresponding author. Address: Department of Anatomy and Neuroscience, Hyogo College of Medicine, 1-1 Mukogawa-cho, Nishinomiya, Hyogo 663-8501, Japan. Tel.: +81 798 45 6416; fax: +81 798 45 6417.
E-mail address: tfukuoka@hyo-med.ac.jp (T. Fukuoka).

0304-3959/$36.00
doi:10.1016/j.pain.2011.09.009

physiologic activity, voltage-gated sodium channels (VGSCs) are the main contributors of the generation and propagation of action potentials. Each VGSC comprises a primary functional component, an α-subunit (Nav), and one or more auxiliary β-subunit(s). Among the nine cloned Navs (Nav1.1–Nav1.9) [18], Nav1.3 is considered to mediate spontaneous discharges because this subtype is normally expressed at low levels by DRG neurons and is dramatically up-regulated after nerve injury [4,7,45]. However, spontaneous discharges are also recorded from the L4 dorsal root in this model [4,27,31]. Therefore, if the L4 DRG contains injured neurons, it is necessary to distinguish injured from spared neurons and to compare the phenotypic changes in Navs.

Another issue is the up-regulation of Nav1.8 in the L4 DRG after L5 SNL. Although reverse transcription-polymerase chain reaction (RT-PCR) studies indicate up-regulation of some Nav mRNAs, including Nav1.8, in the L4 DRG [3,4], immunohistochemical studies have failed to detect an increase in the percentage of Nav1.8-immunoreactive neurons [8,25]. This may be because changes in immunostaining of individual neurons are not always quantifiable using immunohistochemistry. In addition, the expression of Nav mRNAs is significantly different between A-fiber and C-fiber neurons [12]. This may further complicate the evaluation of phenotypic changes in the L4 DRG after L5 SNL.

To address these issues, we have identified ATF3+ (injured) and ATF3− (spared) nuclei among N52+ (A-fiber) and N52− (C-fiber) L4 DRG neurons by double immunostaining, and have objectively compared the expression levels of NPY, several Navs, and BDNF mRNAs in the individual neurons using *in situ* hybridization histochemistry.

2. Materials and methods

2.1. Animals and surgical procedures

A total of 34 young adult male Sprague–Dawley rats weighing 220–230 g (Nippon Animal Co, Nishinomiya, Japan) were used. These rats were housed under controlled temperature and 12-hour light/dark cycle. Food and water were provided *ad libitum*. All care and handling and surgical procedures were approved by the Committee on Animal Research of Hyogo College of Medicine and were performed strictly in accordance with the guidelines of the IASP [48].

All surgical procedures were performed under adequate anesthesia with sodium pentobarbital (50–60 mg/kg, i.p.). To minimize the influence of infection, the hair of the lower back was shaved and the skin was sterilized with 0.5% chlorhexidine and the body was covered with clean paper except for the surgical area. Using sterilized surgical instruments, an approximately 2-cm-long skin incision was made in the midline at the low back level, and the muscles were separated from the spinal process and vertebral arch on the left side at the L6 level. Special care was taken to minimize muscle separation at the more rostral level than the L5/6 zygapophysial joint. After removal of the L6 transverse spinal process, the L5 spinal nerve was identified and ligated tightly with a 4-0 silk suture. In sham-operated rats, the left L5 spinal nerve was isolated, without ligation. In each group, the ipsilateral L4 spinal nerve remained untouched, and the right side was not subjected to any surgery. The wound was washed with 5 mL of distilled saline, and muscle and skin were sutured in two distinct layers with 3-0 silk suture.

2.2. Behavioral tests

The mechanical and thermal sensitivities of the plantar surface of the bilateral hind paws were tested on all animals before, and 1, 3, 7, and 28 days after surgery until sacrifice to verify the successful neuropathic surgery. In addition, other six sham-operated animals were also tested for 7 days (Fig. 1). The withdrawal latency to a radiant heat and mechanical withdrawal threshold were automatically measured using a plantar test (model 7370; Ugo Basile, Comerio, Italy) and a dynamic plantar aesthesiometer (model 37450; Ugo Basile), respectively. Direct behavioral comparison was performed between the first 7 days of eight SNL rats (survived for 7 days and 28 days after surgery, n = 4 each) and six sham-operated rats. The mean value of three trials with at least 5-minute intervals was taken. Data are expressed as mean ± SEM. Differences in the values over time were tested using one-way repeated measures analysis of variance (ANOVA), followed by Bonferroni's multiple comparison test.

2.3. Tissue preparation

At days 1, 3, 7, and 28 after SNL or at days 3 and 7 after sham surgery, rats were deeply anesthetized with sodium pentobarbital (75 mg/kg, i.p.) and killed by decapitation. Bilateral L4 DRGs were freshly harvested, frozen in powdered dry ice, cut into 8-μm-thick serial sections at −20°C, and thaw-mounted onto MAS-coated glass slides (Matsunami, Osaka, Japan). To compare the phenotypic change under the same histochemical condition as possible, the sections, which should be directly compared with each other, were mounted on the same slide. Thus, the slides for the time course experiment (Fig. 2) contained the ipsilateral or contralateral L4 sections obtained from 20 rats sacrificed at different periods (naïve and postoperative days 1, 3, 7, and 28; n = 4 each). The slides for other experiments contained naïve L4, bilateral L4 from sham

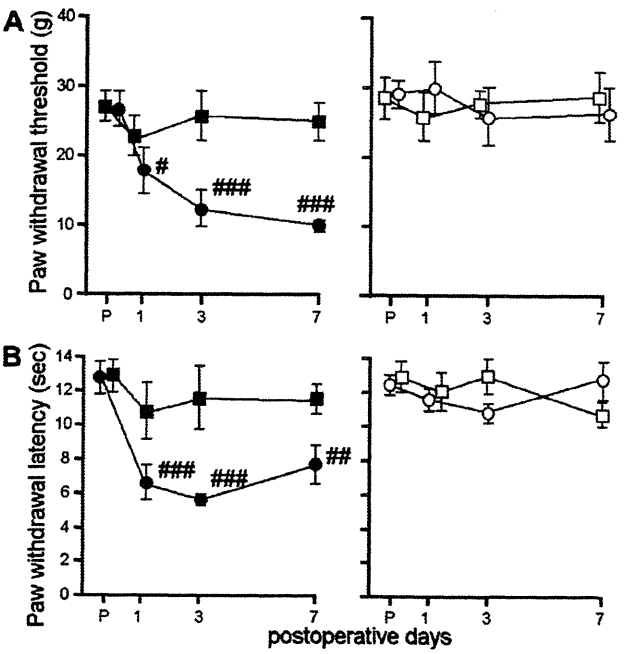

Fig. 1. L5 spinal nerve ligation but not sham operation induces mechanical and thermal hypersensitivity in the ipsilateral hind paw. Paw withdrawal threshold (A) and paw withdrawal latency (B) of the plantar surface were measured by an automatic pinpoint pressure apparatus and a plantar test, respectively, just before (P), 1, 3, and 7 days after sham operation (square, n = 6) or L5 spinal nerve ligation (SNL, n = 8, circle). The closed and open symbols represent ipsilateral and contralateral side, respectively. Error bars = SEM. Mechanical allodynia (drop in threshold) and thermal hyperalgesia (drop in latency) were observed in the ipsilateral side after SNL ($P < .05$, by repeated measures ANOVA), but not after sham operation ($P > .05$). $^{\#}P < .05$, $^{\#\#}P < .01$, $^{\#\#\#}P < .001$ vs P by Bonferroni's multiple comparison test.

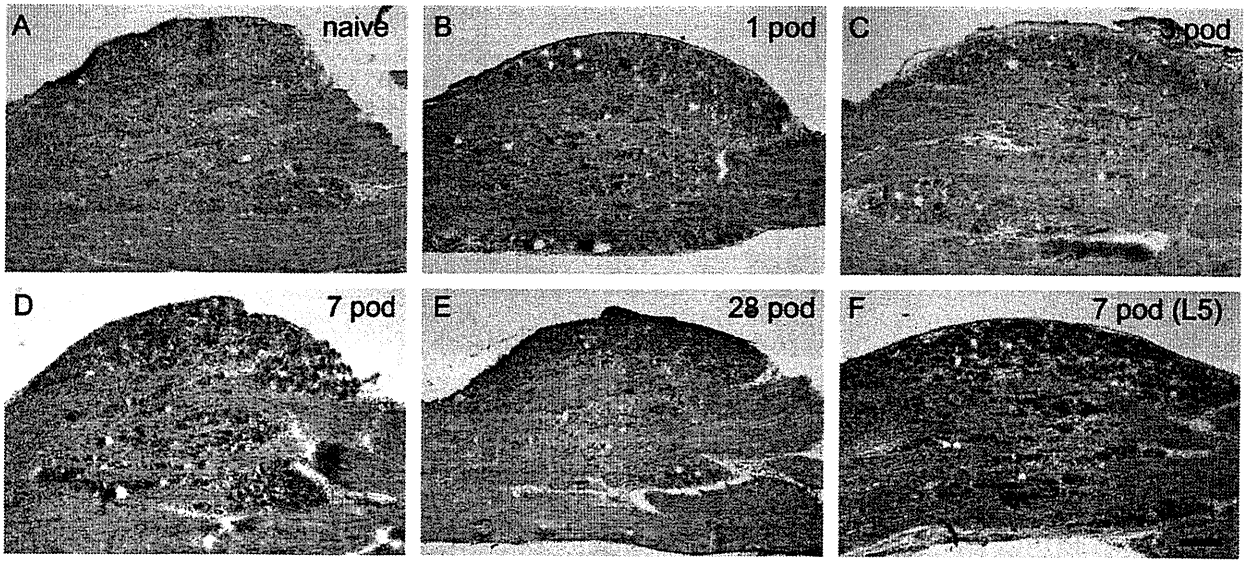

Fig. 2. L5 spinal nerve ligation induces ATF3-immunoreactivity in a limited number of ipsilateral L4 DRG neurons. The ipsilateral L4 DRG sections obtained from naive rats or animals received L5 SNL at the indicated days before (pod; post-operative day) were mounted on a slide grass and processed for immunohistochemistry for ATF3 under the same condition. There were no detectable ATF3+ nuclei in the naive L4 DRG (A). Several ATF3+ nuclei (brown) were observed by the first day (B) and remained throughout the experiment (E; 28 pod). The ipsilateral L5 DRG contained numerous ATF3+ nuclei (F) 7 days after L5 SNL. Scale bar, 100 μm.

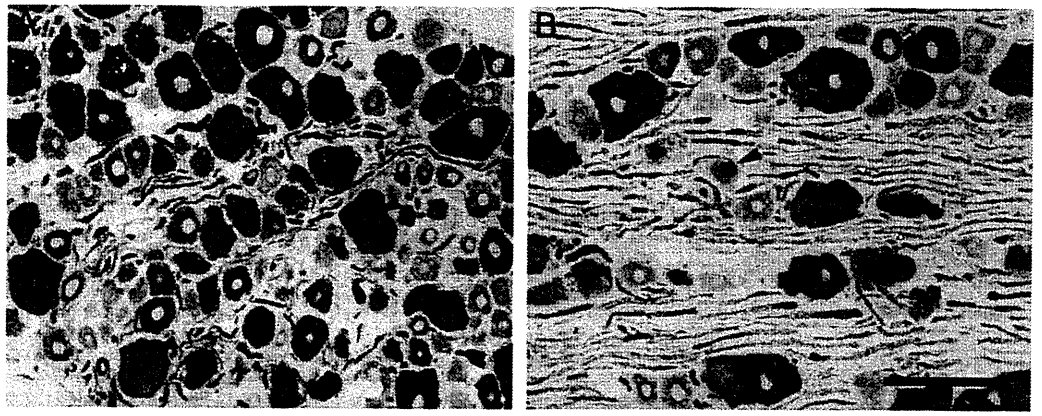

Fig. 3. ATF3 is induced mainly in myelinated afferent neurons in the ipsilateral L4 DRG 3 days after L5 SNL. Double immunostaining of the ipsilateral L4 DRG sections using a rabbit polyclonal antibody for ATF3 (black in the nucleus) and a monoclonal antibody (clone N52) for phosphorylated/non-phosphorylated neurofilament of MW 200 kDa (brown in the cytoplasm) were performed. (A) Three N52+ neuronal profiles containing ATF3+ nuclei are indicated by arrowheads. Note that most neuronal nuclei were not immunostained. (B) Example of an ATF3+ nucleus in a N52− neuronal profile is indicated by arrowhead. Scale bar, 100 μm.

and SNL rats 3 or 7 days after surgeries (n = 4 each). These time points were selected because (1) neuropathic pain behaviors are fully developed around days 3 (Fig. 1), so phenotypic changes that contribute to the pain behaviors should occur by this time point; and (2) most of the previous histochemical studies are performed at day 7, making comparisons easier. Either data set is presented according to other conditions as described in the Results section. Similarly processed L5 DRG sections were used as positive control for injury-induced phenotypic changes (Figs. 2F and 4B). Sections were stored at −80°C until use.

2.4. Immunohistochemistry

The freshly frozen tissue sections were air-dried at room temperature (RT), fixed in 4% formaldehyde (FA) in 0.1 mol/L phosphate buffer (PB) for 20 minutes After three 5-minutes washes in Tris-buffered saline (TBS), the sections were blocked for 30 minutes in TBS containing 10% normal goat serum (NGS), and incubated at 4°C for 18 hours with rabbit anti-ATF3 antibody (1:200, C-19; Santa Cruz Biotechnology, Santa Cruz, CA) in TBS containing 5% NGS. After washing in TBS three times each for 5 minutes, biotinylated goat anti-rabbit IgG antibody (1:200, Vector Laboratories, Burlingame, CA) was applied for 2 hours. Next, endogenous peroxidase was quenched with a 15-minute wash in TBS containing 0.1% H_2O_2 and 30% methanol. The slides were rinsed in TBS, followed by incubation in avidin–biotin–peroxidase complex (Elite ABC kit; Vector Laboratories) for 30 minutes at RT. The horseradish peroxidase reaction was developed in TBS containing 0.05% diaminobenzidine (Wako, Tokyo, Japan), and 0.01% H_2O_2. Some sections were immunostained by N52, a widely used monoclonal antibody against the 200-kDa neurofilament subunit (Sigma, St. Louis, MO) [39,42], which stains neuronal cell bodies with myelinated axons, before ATF3 immunohistochemistry. In that case, 0.3% nickel sulfate was added to the above mentioned final peroxidase reaction for ATF3, and N52 was applied at 1:20,000 for 30 minutes at RT as a primary antibody and biotinylated horse anti-mouse IgG

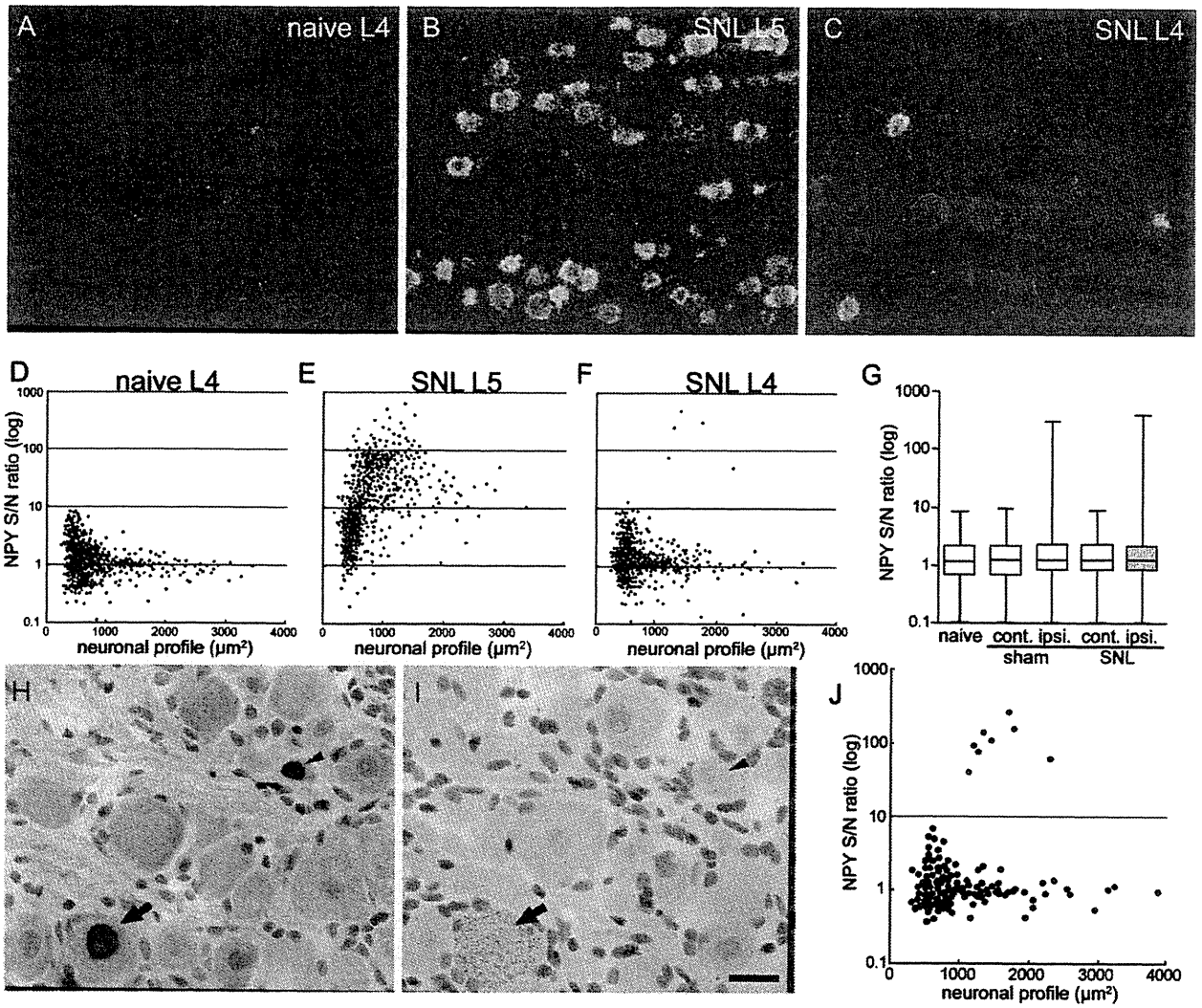

Fig. 4. ATF3+ large neurons in the ipsilateral L4 DRG begin to express NPY mRNA following L5 SNL. (A–C) Dark-field view of naïve L4 (A), ipsilateral L5 (B) and L4 (C) DRG sections processed for *in situ* hybridization for NPY mRNA 3 days after L5 SNL. Some neurons were clearly labeled for NPY in the L4 DRG. Scale bar, 100 μm. (D–F) Scatterplot diagrams showing the signal intensities (S/N ratio in log scale) for NPY mRNA and cell size in naïve L4 (D), the ipsilateral L5 (E), and the ipsilateral L4 (F) DRG sections 7 days after L5 SNL. At least 269 neuronal profiles pooled from four rats were plotted. There were a limited number of neurons strongly labeled for NPY in the SNL L4 DRG as compared with naïve L4. (G) Box-and-whisker plots showing the distribution of NPY S/N ratios of naïve L4 DRG and the ipsilateral (ipsi.) and the contralateral (contra.) L4 DRGs obtained from sham-operated and L5 SNL rats (n = 269–370 neuronal profiles pooled from four rats in each group). The whiskers indicate the maximum and minimum values, and the box indicates upper quartile, median and lower quartile. Since the positively-labeled profiles were rare in number, there were no significant differences among the groups ($P > .05$ by Kruskal–Wallis test). (H and I) Two serial sections of the ipsilateral L4 DRG processed for ATF3-immunoreactivity (H) and *in situ* hybridization for NPY mRNA (I). The arrow indicates double-labeled large neurons. The arrowhead indicates ATF3+ small neurons with just detectable accumulation of silver grains. Scale bar, 25 μm. (J) Representative scatterplot showing S/N ratios for NPY mRNA in ATF3+ (red dots) and ATF3− neurons (black dots) in the ipsilateral L4 DRG 7 days after SNL. Only ATF3+ neurons were positively labeled for NPY.

antibody (1:200, Vector Laboratories) was used as a secondary antibody. Normal horse serum was used instead of NGS, and the final development was carried out without nickel sulfate. These slides were dehydrated in a graded ethanol series, cleared in xylene, and coverslipped.

2.5. In situ hybridization histochemistry (ISHH)

Partial cDNAs of rat Nav1.1, Nav1.3, Nav1.6, Nav1.7, Nav1.8, Nav1.9, and BDNF were cloned previously [12,34]. Partial cDNA of rat NPY (GenBank Accession No. M20373; base 42–430) was synthesized by RT-PCR from rat DRG-derived total RNA, cloned into p-GEM T-easy vector (Promega, Madison, WI) and sequenced as described previously [12]. These vectors were digested by a restriction enzyme SpeI or NcoI (Takara Bio, Otsu, Japan) in adequate buffer, and alpha ^{35}S UTP-labeled antisense and sense cRNA probes were synthesized using T7 or SP6 RNA polymerase (Promega). These probes were mixed at 10^4 cpm/μL in hybridization buffer (50% deionized formamide, 0.3 mol/L NaCl, 20 mmol/L Tris–HCl [pH 7.5], 5 mmol/L ethylenediaminetetraacetic acid [EDTA; pH 8.0], 10% dextran sulfate, 1× Denhardt's solution, 0.2% sarcosyl, 250 μg/mL yeast tRNA, 400 μg/mL salmon testis DNA, and 20 mmol/L dithiothreitol [DTT: pH 8.0]), applied at a 200-μL volume to the section, and then incubated at 55°C overnight in a humidified box. Following hybridization, these sections received a 30-minute wash at 60°C in 2× standard saline citrate (SSC: 1× SSC is 150 mmol/L NaCl and 15 mmol/L sodium citrate, pH 7.0) containing 5 mmol/L DTT, a 30-minute wash in 50% formamide, 2× SSC containing 5 mmol/L DTT, treated with 1 μg/mL RNase A (Roche, Mannheim, Germany) in RNase buffer [0.5 mol/L NaCl, 10 mmol/L Tris–HCl, and 1 mmol/L EDTA (pH 7.5)] for 30 minutes at 37°C, washed in 50% formamide, 2× SSC containing 5 mmol/L

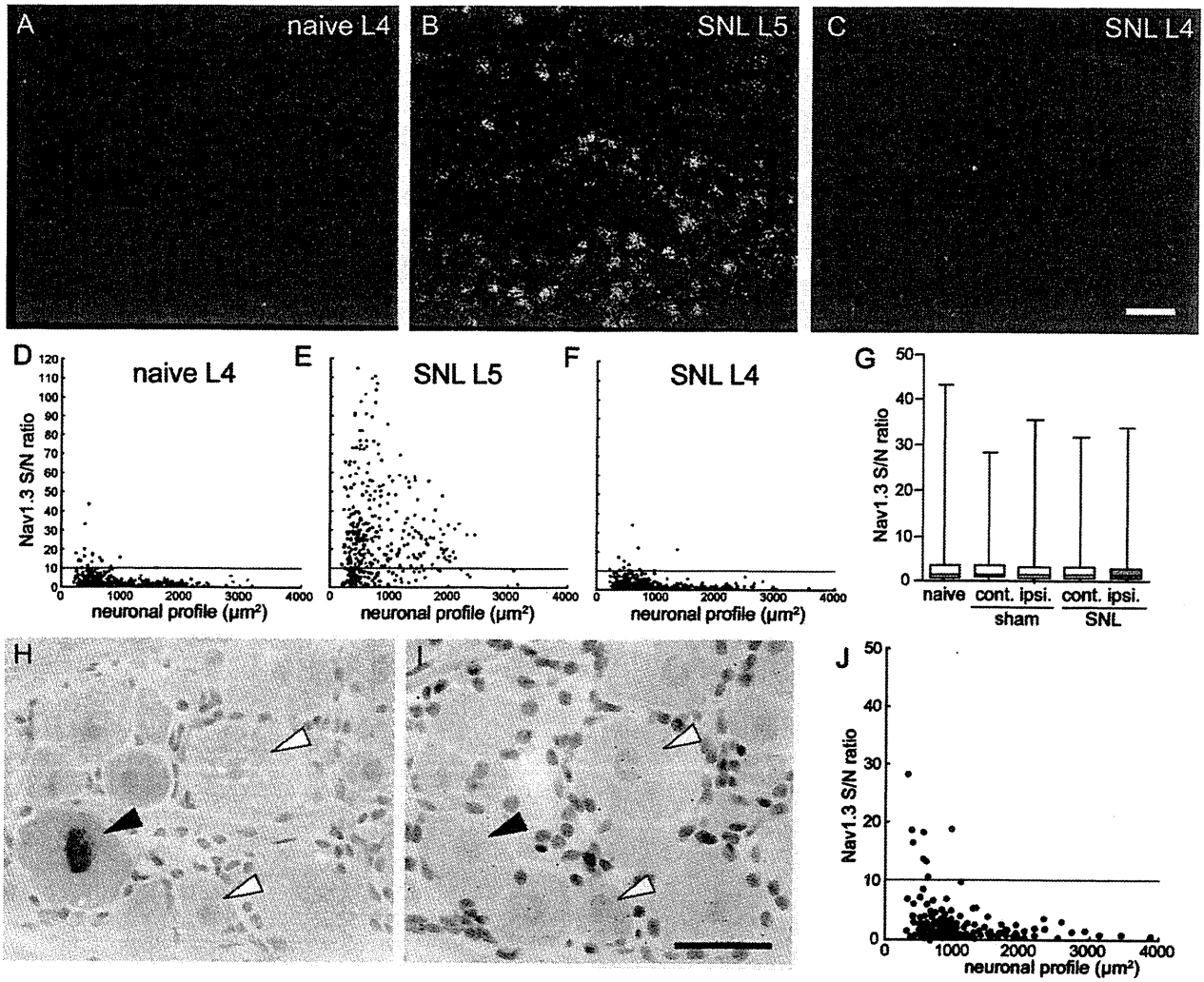

Fig. 5. No apparent induction of Nav1.3 mRNA in the ipsilateral L4 DRG following L5 SNL. (A–C) Dark-field photomicrographs showing ISHH signals for Nav1.3 mRNA in naïve L4 (A), the ipsilateral L5 (B), and the ipsilateral L4 (C) DRG sections obtained from rats that received L5 SNL 7 days before. The L5 DRG displayed large increases in signals for Nav1.3 mRNA, while the L4 DRG showed no obvious change as compared with naïve L4 DRG. Scale bar, 100 μm. (D–F) Scatterplot diagrams showing the signal intensities (S/N ratio) for Nav1.3 mRNA and cell size in naïve L4 (D), the ipsilateral L5 (E) and the ipsilateral L4 (F) DRG sections 7 days after L5 SNL. At least 300 neuronal profiles pooled from four rats were plotted. Note that there was no up-regulation of Nav1.3 signal in the SNL L4 DRG as compared with naïve L4. (G) Box and whisker plots showing the distribution of Nav1.3 S/N ratios of naïve L4 DRG and the ipsilateral (ipsi.) and the contralateral (contra.) L4 DRGs obtained from sham-operated and L5 SNL rats (n = 278–389 neuronal profiles pooled from four rats in each group). The whiskers indicate the maximum and minimum values, and the box indicates upper quartile, median and lower quartile. Since so many S/N ratios are near "0" (D and F), the lower whiskers are short. No significant differences were observed among the groups ($P > .05$ by Kruskal–Wallis test). (H and I) Bright-field photomicrographs of the serial L4 DRG sections 7 days after SNL processed for ATF3-immunostaining (H) and ISHH for Nav1.3 mRNA (I). Note that ATF3+ cell (black arrowhead) and ATF3− cells (white arrowheads) are similarly labeled for Nav1.3. (J) Representative scatterplot showing S/N ratios for Nav1.3 mRNA in ATF3+ (red dots) and ATF3− neurons (black dots) in the ipsilateral L4 DRG 7 days after SNL.

DTT for 30 minutes at 60°C, rinsed in 1× SSC and 0.1× SSC for 10 minutes at RT each, dehydrated through an ascending ethanol series, and air dried. For autoradiography, these sections were dipped in NTB emulsion (Eastman Kodak, Rochester, NY) diluted 2:3 with distilled water at 45°C and exposed for overnight (NPY) or 2–4 weeks (others) at 4°C. Following development in D-19 (Eastman Kodak) and fixation in 24% sodium thiosulfate, the sections were counterstained with hematoxylin and eosin, dehydrated in a graded ethanol series, cleared in xylene, and coverslipped.

2.6. Data analysis

Sections were viewed on a microscope (Diaphot 300, Nikon, Tokyo, Japan) under bright- or dark-field illumination, captured with a digital camera (DXM-1200, Nikon) and ACT-1 software, and saved as TIFF files in a computer. The proportion of ATF3+ DRG cells was determined by manual counting of the number of ATF3+ nuclei (brown in Figs. 2, 4 and 5, and black in Figs. 3 and 7–9) and ATF3− nuclei (light purple in Figs. 2, 4 and 5, and white in Figs. 3 and 7–9) of all neuronal profiles in a DRG section from each side of each rat (n = 4 at each time point). All neuronal profiles that did not contain visible nuclei were omitted. The percentages of positively labeled profiles were calculated and expressed throughout as mean ± SEM (n = 4). The changes in the percentages were analyzed using one-way ANOVA followed by Dunnett's multiple comparison test (Table 1).

To compare ISHH signals over individual neuronal profiles in the total neuronal populations (Figs. 4D–G, 5D–G, 6, and 9D), we analyzed all neuronal profiles containing visible nuclei in a randomly selected tissue section from each rat (n = 4).

For colocalization analysis, we manually identified all neuronal profiles sectioned into the serial tissue sections (Figs. 4H–J, 5H–J, 7

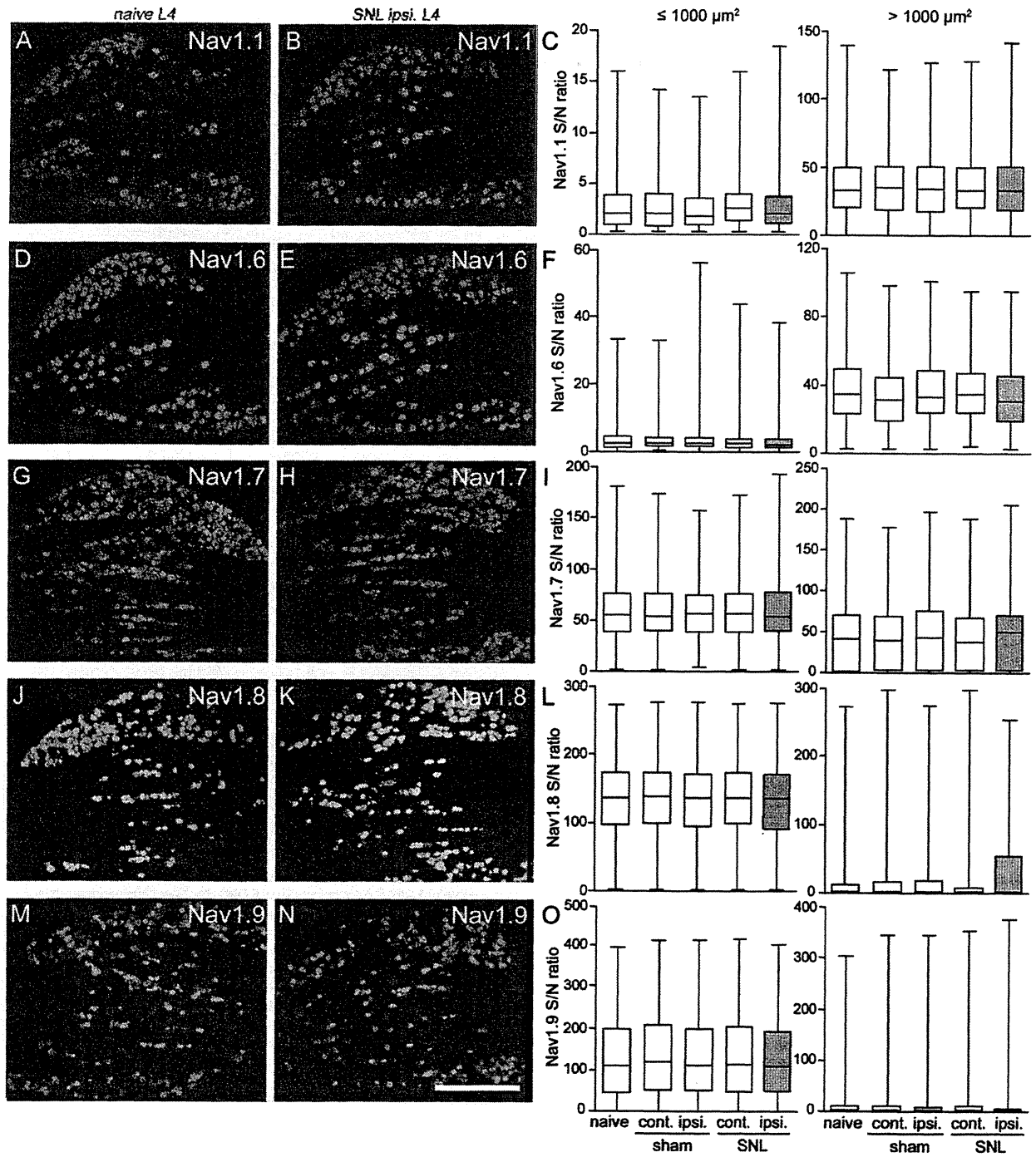

Fig. 6. Changes in expression for Nav mRNAs in the L4 DRG 3 days after L5 SNL. Dark-field photomicrographs showing ISHH signals for Nav1.1 (A and B), Nav1.6 (D and E), Nav1.7 (G and H), Nav1.8 (J and K), and Nav1.9 (M and N) mRNAs in naïve (A, D, G, J, and M) and the SNL ipsilateral L4 (B, E, H, K, and N) DRGs. Scale bar = 500 μm. No apparent differences could be detected by subjective observation. (C, F, I, L, and O) Box-and-whisker plots showing the distribution of Nav S/N ratios of naïve L4 DRG and the ipsilateral (ipsi.) and contralateral (contra.) L4 DRGs obtained from sham-operated and L5 SNL rats (n > 100 neuronal profiles for C, F, and I, n > 400 neuronal profiles for L and O pooled from four rats in each group). The whiskers indicate the maximum and minimum values, and the box indicates upper quartile, median and lower quartile. No significant differences were observed between any combinations ($P > .05$ by Kruskal–Wallis test or Mann–Whitney test).

and 8, and 9E–G). Because small neurons are sectioned into fewer profiles than larger neurons during cryostat sectioning, small neuronal profiles are often identified in only one of the serial sections, and these profiles were omitted from the colocalization analysis. We did not apply the cell count correction used in our previous studies [12,24]. Therefore, overall neuronal sample should contain more large cells than the representative size distribution of DRG neurons.

For image analysis of the sections processed for ISHH, we analyzed the density of silver grains over the neuronal profiles using a computerized image analysis system (NIH Image, version 1.61), as described before [12]. The percentage of grain-occupied area

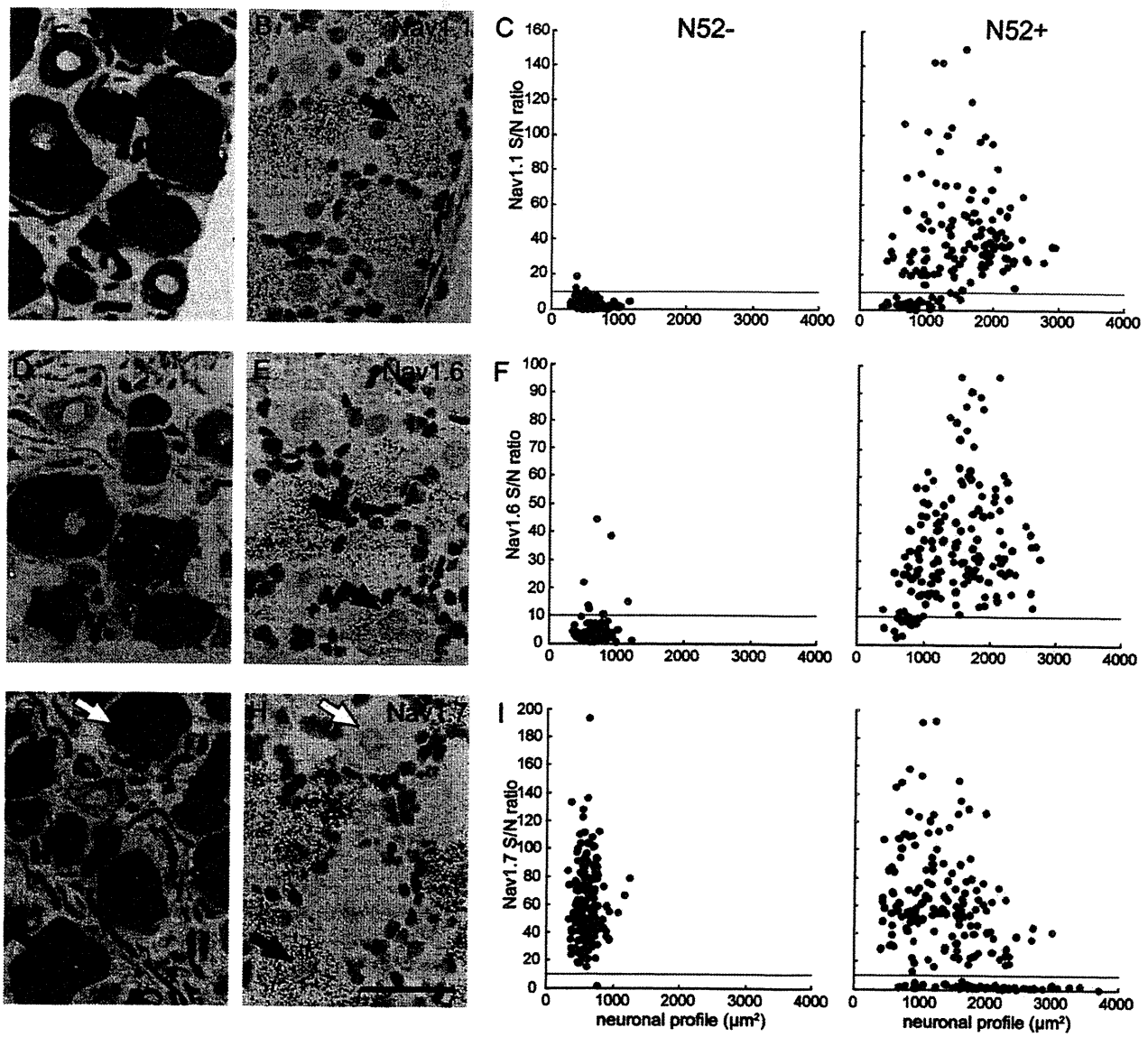

Fig. 7. TTX-s Nav mRNAs persist in the injured L4 DRG neurons 3 days after L5 SNL. Serial tissue sections (A and B, D and E, and G and H) were processed for double immunostaining for ATF3/N52 (A, D, and G) and *in situ* hybridization for Nav1.1 (B), Nav1.6 (E), and Nav1.7 (H). Scale bar, 50 μm. Arrows indicate ATF3+ profiles. S/N ratios for Nav1.1 (C), Nav1.6 (F), and Nav1.7 (I) of N52− and N52+ neuronal profiles were measured and presented as scatterplots. Red and black dots indicate ATF3+ (injured) and ATF3− (spared) profiles, respectively.

of each neuronal profile was divided by the background grain density giving a signal/noise (S/N) ratio. The S/N ratios of individual neurons versus their cross-sectional areas were plotted as scattergrams, or the distribution of the S/N ratio was presented as box and whisker plots. We defined an S/N ratio = 10 as the borderline between positively and negatively labeled neurons for the corresponding transcript. For each sense probe, S/N ratios of at least 100 randomly selected neuronal profiles were distributed between 0.78 and 1.58. Because the distribution of S/N ratio could not be assumed to follow a Gaussian distribution, the signal intensities among naïve DRG and either side of DRG from sham-operated and SNL rats were analyzed using the Kruskal–Wallis test followed by Dunn's multiple comparison test. Comparison between the ipsilateral side and the contralateral side and between ATF3+ and ATF3− populations in the ipsilateral DRG from SNL rats were analyzed using the Mann–Whitney U test.

We applied similar image analysis for quantification of the N52-immunostaining and defined the profiles with immunoproduct occupying more than 20% of the cytoplasm cross-sectional area (without the nucleus) as positively labeled by N52 (N52+) as described previously [14].

All statistical calculations were performed using Prism4 (GraphPad Software, San Diego, CA).

3. Results

3.1. Behavioral tests

Animals having undergone unilateral L5 SNL developed a significant decrease in withdrawal threshold in the ipsilateral hindpaw at day 1 ($P < .05$ by repeated measures ANOVA followed by Bonferroni's multiple comparison test) compared with the preoperative value. The threshold further decreased at day 3 ($P < .001$), and continued at a similar level at least until day 7 (Fig. 1A). The withdrawal latency to heat stimuli rapidly decreased to minimal value at day 1 ($P < .001$) and continued depressed throughout the

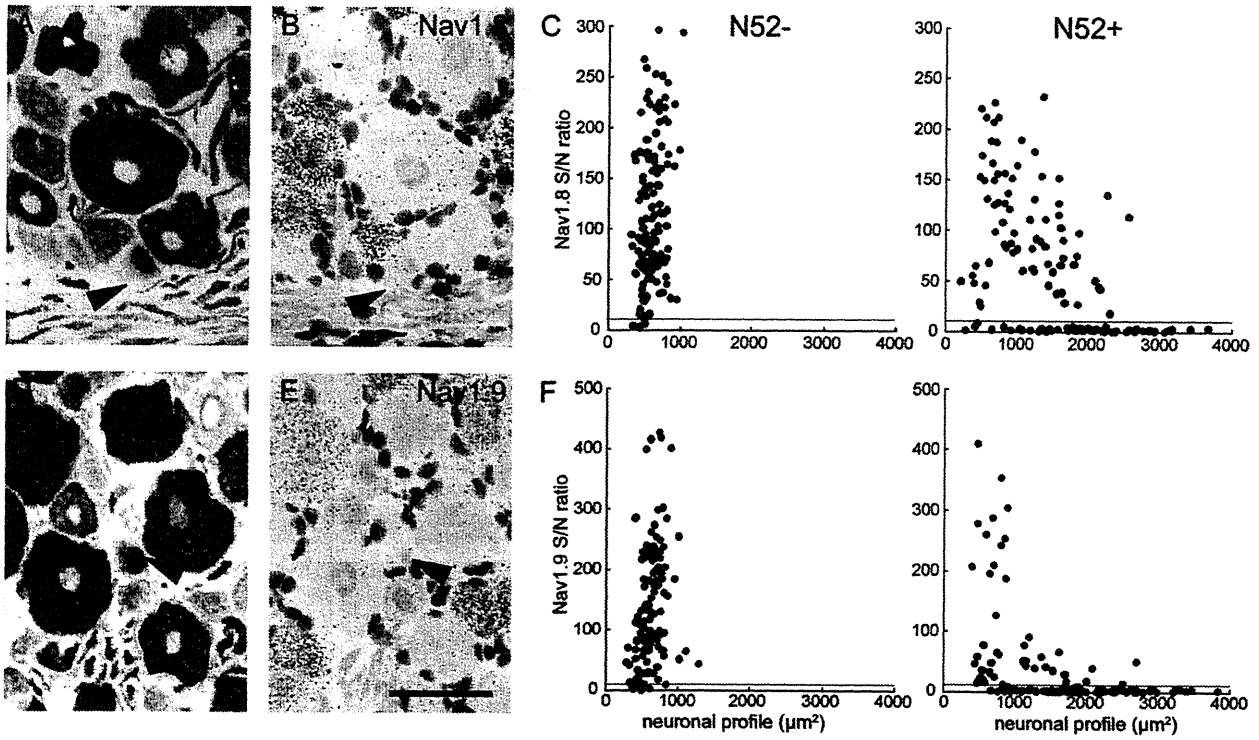

Fig. 8. TTX-r Nav mRNAs decrease in the injured C-fiber neurons in the L4 DRG 3 days after L5 SNL. Serial tissue sections (A and B, D and E) were processed for double immunostaining for ATF3/N52 (A and D) and *in situ* hybridization for Nav1.8 (B) and Nav1.9 (E). Scale bar, 50 μm. Arrowheads indicate ATF3+ profiles. S/N ratios for Nav1.8 (C) and Nav1.9 (F) of N52− and N52+ neuronal profiles were measured and are presented as scatterplots. Red and black dots indicate ATF3+ (injured) and ATF3− (spared) profiles, respectively. Note that the N52−/ATF3+ cells had relatively low signals for Nav1.8 and Nav1.9.

examined period in the ipsilateral hind paw of L5 SNL rats (Fig. 1B). In contrast, sham-operated animals did not display significant changes in these behavioral tests. There were no significant changes in the contralateral side after either surgery.

3.2. There was only a limited number of neurons having ATF3+ nuclei in the ipsilateral L4 DRG after L5 SNL

No ATF3+ nuclei were observed in the naïve L4 DRG (Fig. 2A, 0 of 1200 counted nuclei). After L5 SNL, the ipsilateral L5 DRG contained numerous ATF3+ nuclei (Fig. 2F). ATF3+ nuclei were observed in a very limited proportion of the ipsilateral L4 neuronal nuclei from day 1 to day 28 after SNL (Fig. 2B–E). The proportions of ATF3+ nuclei in the ipsilateral L4 DRG were significantly higher than naïve value (0%) from day 3 to day 28 (Table 1). Although many fewer ATF3+ nuclei were also observed in the contralateral L4 DRG, these percentages did not reach a significant value ($P = .34$ by one-way ANOVA). The percentages in the ipsilateral L4 DRGs were not significantly different between L5 SNL rats and sham-operated rats at day 3 ($5.7 \pm 0.6\%$ vs $4.1 \pm 0.5\%$, $n = 4$, $P > .05$ by unpaired t test). This was also the case for the contralateral side.

3.3. ATF3+ neurons in A-fiber and C-fiber populations

To compare the directly injured proportions between A-fiber (N52+) and C-fiber (N52−) neurons, we performed double immunohistochemistry for ATF3 in the nuclei (black) and N52 in the cytoplasm (brown) (Fig. 3). As we reported previously [12], because N52-immunostaining of the directly injured cell bodies 7 days after SNL was somewhat degraded, we presented the data from the rats underwent SNL 3 days before to avoid misclassification of the limited number of injured L4 neurons. We analyzed 1105 N52+ neurons and 880 N52− L4 DRG neurons from four SNL rats. Among the nuclei of N52− neurons, only $1.6 \pm 0.6\%$ were ATF3+ (arrowhead in Fig. 3B) and this value was significantly lower than that of N52+ neurons (arrowheads in Fig. 3A, $4.7 \pm 0.9\%$, $P < .001$ by paired t-test).

3.4. Up-regulation of NPY mRNA by injured large neurons in the ipsilateral L4 DRG

NPY is strongly up-regulated by DRG cells after axonal injury [35]. Because we found a limited number of ATF3+ cells in the L4 DRG, we examined whether NPY mRNA was induced in these cells (Fig. 4). Almost no detectable signals were observed in the naïve DRG (Fig. 4A and D). Three days after L5 SNL when ATF3 expression significantly increased in the L4 DRG (Table 1), many L5 DRG neurons, mainly large ones, clearly increased the expression of NPY mRNA (Fig. 4B and E). At the same time point only a very few L4 DRG neurons were clearly labeled for NPY mRNA (Fig. 4C and F). Such positively labeled neurons occupied only $0.7 \pm 0.2\%$ and $0.8 \pm 0.3\%$ of all counted neurons in the ipsilateral L4 DRG after L5 SNL and sham operation, respectively. There was no significant difference between these values ($P > .05$ by unpaired t-test), and these small numbers of positive neurons did not cause a significant difference in the S/N ratios of the total neuronal population among L4 DRGs of naïve, sham-operated, and SNL rats ($P > .1$ by Kruskal–Wallis test; Fig. 4G). This was also the case for the L4 DRGs 7 days after surgery (not shown). Colocalization study revealed that only ATF3+ large neurons increased NPY in L4 DRG (arrows in Fig. 4H and I and red dots in Fig. 4J). ATF3+ small neurons had only just detectable signals for NPY (arrowheads in Fig. 4H and I), and all

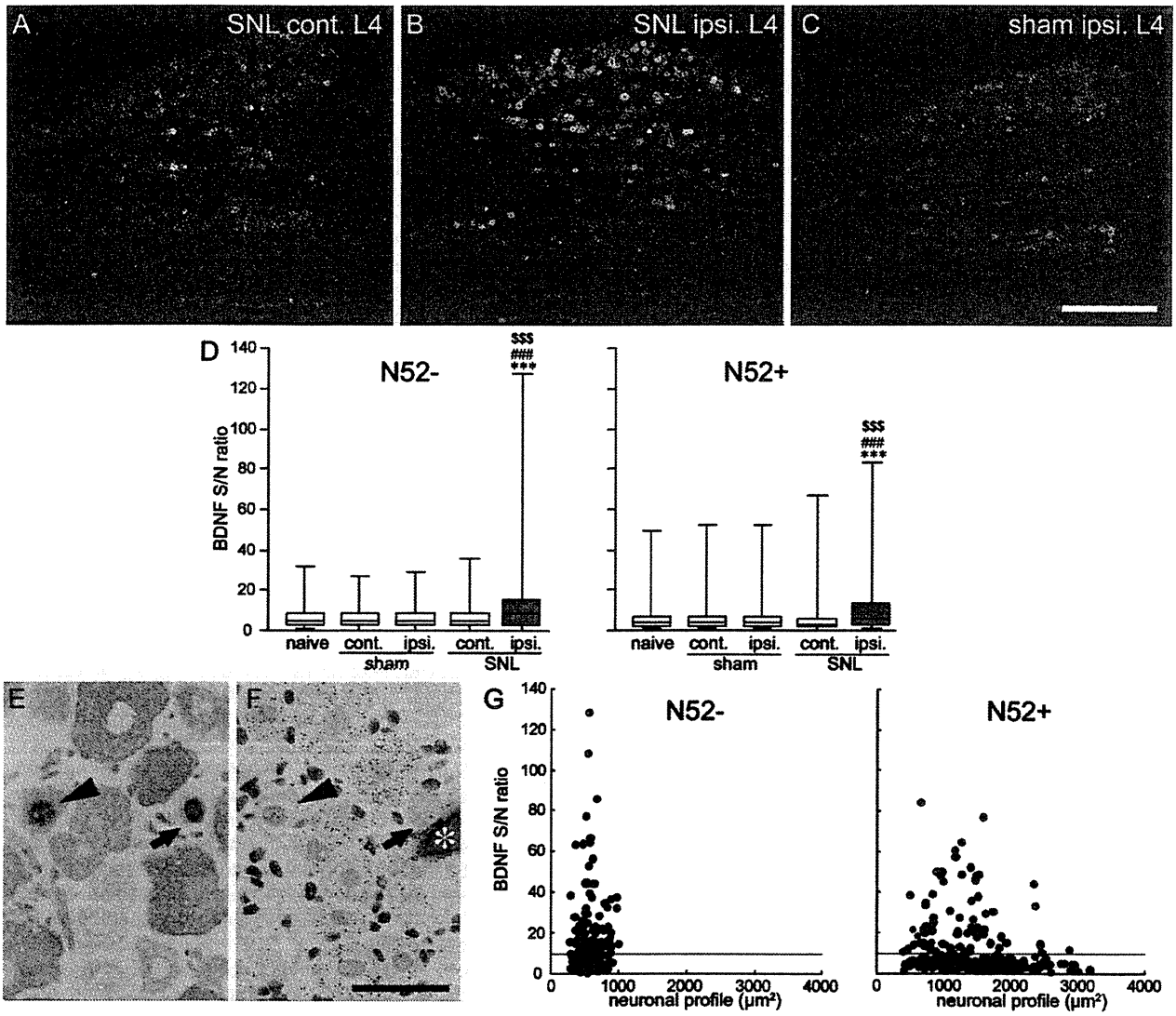

Fig. 9. BDNF increases preferentially in ATF3– L4 DRG neurons following L5 SNL. (A–C) Dark-field photomicrographs showing *in situ* hybridization signals for BDNF in the L4 DRG sections on the contralateral (A) and ipsilateral side (B) 3 days after L5 SNL and on the ipsilateral side (C) 3 days after sham surgery. L5 SNL, but not sham surgery, increased BDNF mRNA in the ipsilateral L4 DRG. Scale bar, 500 μm. (D) Box and whisker plots showing BDNF S/N ratio of N52– and N52+ neuronal populations in naïve L4 DRG, and ipsilateral (ipsi.) and contralateral (contra.) L4 DRGs obtained from sham-operated and L5 SNL-operated rats (n = 217–239 neuronal profiles pooled from four rats in each group). The whiskers indicate the maximum and minimum values, and the box indicates upper quartile, median and lower quartile. $^{\$\$\$}P < .001$ vs naïve, $^{***}P < .001$ vs the same side of sham-operated rats by Kruskal–Wallis test followed by Dunn's multiple comparison test. $P < .001$ vs contralateral side by Mann–Whitney test. (E and F) Serial sections of the ipsilateral L4 DRG harvested from rats that received L5 SNL 3 days before were processed for double immunostaining for ATF3 (black nuclei) and N52 (brown cytoplasm) (E) and *in situ* hybridization for BDNF (F). Scale bar, 50 μm. Note that ATF3+ neurons have relatively low signals (arrow and arrowheads). Asterisk (*) in F indicates debris. (G) Scatterplot diagrams showing the S/N ratios for BDNF of N52– and N52+ cells in the ipsilateral L4 DRG following L5 SNL. Black and red dots indicate spared (ATF3–) and injured (ATF3+) neuronal profiles, respectively. Note that the spared neurons have relatively higher S/N ratios than injured neurons.

Table 1
Percentage of ATF3-immunoreactive nuclei in the L4 dorsal root ganglion after unilateral L5 spinal nerve ligation.

	Naive	L5 spinal nerve ligation				Sham
		1 POD	3 POD	7 POD	28 POD	3 POD
Ipsilateral	0	3.6 ± 1.6	5.7 ± 0.6*	6.0 ± 1.8**	4.7 ± 0.9*	4.1 ± 0.5
Contralateral	0	0.9 ± 0.5	1.5 ± 1.0	0.3 ± 0.2	0.6 ± 0.3	1.6 ± 1.3

Data are expressed as mean ± SEM (n = 4).
POD, postoperative days.
*$P < .05$, **$P < .01$ vs. naive by one-way analysis of variance followed by Dunnett's multiple comparison test.

ATF3− neurons were not labeled (S/N ratio <10) for NPY (black dots in Fig. 4J).

3.5. Minor induction of Nav1.3 in the ipsilateral L4 DRG

Nav1.3 is maximally up-regulated 7 days after sciatic nerve injury by the axotomized DRG neurons [45]. This is also the case for the injured L5 DRG after L5 SNL (Fukuoka, unpublished data). Because we found some ATF3+ neurons in the ipsilateral L4 DRG (Fig. 2), we examined the change in expression of this channel. The Nav1.3 signals were almost undetectable in naïve DRG (Fig. 5A and D). L5 SNL led to a large increase in Nav1.3 expression by L5 DRG neurons 7 days after SNL (Fig. 5B and E). In contrast, no detectable change in Nav1.3 expression was observed in the L4 DRG at the same time point (Fig. 5C and F), and there was no significant difference in S/N ratios of the total neuronal population among L4 DRGs of naïve, sham-operated, and SNL rats ($P > .1$ by Kruskal–Wallis test; Fig. 5G). This was also the case throughout the examined periods (postoperative day 1–28; data not shown). We further compared the S/N ratios for Nav1.3 of ATF3+ and ATF3− neurons in the SNL ipsilateral L4 DRG (Fig. 5H–J). We identified 21 ATF3+ neurons and 75 ATF3− neurons, and compared their S/N ratios. Most ATF3+ neurons (black arrowhead in Fig. 5I) had just detectable signals for Nav1.3 mRNA similar to ATF3− neurons (white arrowheads in Fig. 5I) in contrast with the ipsilateral L5 DRG that showed dramatic up-regulation of this transcript (Fig. 5B and E). Indeed, these signals were much less than those of the L5 DRG ($P < .001$ by Mann–Whitney test; Fig. 5E and F). However, direct statistical comparison of S/N ratio of ATF3+ and ATF3− populations in the ipsilateral L4 DRG revealed that ATF3+ neurons had higher S/N ratio than ATF3− neurons (Fig. 5J, $P < .01$ by Mann–Whitney test).

3.6. No significant changes in expression of Nav mRNAs in the total neuronal population of the SNL ipsilateral L4 DRG

Next, we examined whether other Nav mRNAs, especially previously reported Nav1.8, might be up-regulated in the SNL ipsilateral L4 DRG 3 days after surgery when neuropathic pain behaviors were fully developed (Fig. 1). ISHH revealed clear signals for all examined Navs, and no apparent difference was detected between naïve and SNL ipsilateral L4 DRGs under microscopic observation (Fig. 6). Because the normal expression of Nav mRNAs, other than Nav1.3, are significantly different between C-fiber and A-fiber neurons [12], we separated all neuronal profiles with visible nuclei into smaller ($\leqslant 1000\ \mu m^2$) and larger ($>1000\ \mu m^2$) populations and compared S/N ratios for Nav mRNAs using ISHH (Fig. 6). This criterion is based on our previous observations that N52− neurons are exclusively included in the smaller population with some N52+ neurons and that the larger population exclusively contains N52+ neurons [14]. Despite such separation, statistical analysis failed to detect significant changes in either neuronal population for all examined Navs ($P > .05$ by the Kruskal–Wallis test, Fig. 6). Although the larger population in SNL ipsilateral side seemed to have higher signals for Nav1.8 than contralateral side (Fig. 6L), the difference did not reach significance ($P = .152$ by Mann–Whitney test).

3.7. Selective down-regulation of tetrodotoxin-resistant (TTX-r) Nav mRNAs in injured C-fiber neurons in the SNL ipsilateral L4 DRG

We further examined whether Nav mRNAs might change in the limited number of ATF3+ neurons as compared with ATF3− neurons using serial tissue sections 3 days after L5 SNL (Figs. 7 and 8). This time point was chosen because down- or up-regulation of Nav transcripts was evident in the L5 DRG, and N52-immunoreactivity was reduced at longer time points [12]. We found 15 N52−/ATF3+ (injured C-fiber) profiles and 50 N52+/ATF3+ (injured A-fiber) profiles among analyzed 2955 neuronal profiles. As we reported previously [12], N52−/ATF3− (spared C-fiber) neurons in the SNL ipsilateral L4 DRG rarely expressed Nav1.1 or Nav1.6 mRNA, but almost all (>95%) these neurons normally expressed Nav1.7, Nav1.8, and Nav1.9 mRNAs with relatively high signals (black dots in Figs. 7 and 8). N52−/ATF3+ profiles had significantly lower signals for Nav1.8 and Nav1.9 (red dots in Fig. 8) than N52−/ATF3− profiles ($P < .0001$ by the Mann–Whitney U test), whereas there were no significant differences in signal intensities for tetrodotoxin-sensitive (TTX-s) Nav1.1 ($P > .8$), Nav1.6 ($P > .1$), or Nav1.7 mRNA ($P > .1$) between these two populations (Fig. 7).

On the other hand, N52+/ATF3− (spared A-fiber) profiles in the ipsilateral L4 DRG (black dots in Figs. 7 and 8) expressed all of these Nav mRNAs at various rates (Nav1.1, 78%; Nav1.6, 84%; Nav1.7, 73%, Nav1.8, 50%; Nav1.9, 33%). The S/N ratios for all Nav mRNAs of N52+/ATF3+ profiles (red dots in Figs. 7 and 8) were equivalent to those of N52+/ATF3− profiles ($P > .2$–$.9$ by Mann–Whitney U test).

3.8. Spared neurons increase BDNF mRNA in the ipsilateral L4 DRG

Following L5 SNL, expression of BDNF is increased in the ipsilateral L4 DRG [13,19]. On the other hand, BDNF is up-regulated also in the directly injured DRG [29]. Because we found a limited number of ATF3+ L4 DRG neurons in this model (Fig. 2), we verified this up-regulation of BDNF in the SNL ipsilateral L4 DRG and directly compared BDNF expression between injured and frankly spared L4 DRG neurons (Fig. 9). The sensitivity of ISHH in this study using a newly designed riboprobe was greatly improved over that in our previous study using an oligoprobe [13]. BDNF expression clearly increased in the ipsilateral L4 DRG (Fig. 9B) 3 days after SNL, when the neuropathic pain behaviors were fully developed, as compared with the SNL contralateral (Fig. 9A), sham ipsilateral (Fig. 9C), and naïve L4 DRGs (not shown). S/N ratios for BDNF were compared among naïve L4 DRG, bilateral L4 DRGs from sham and SNL rats with separation between N52− and N52+ neuronal populations (Fig. 9D). For both N52− and N52+ populations, S/N ratios were significantly higher in the SNL ipsilateral L4 DRG as compared with those in naïve and the sham ipsilateral L4 DRG ($P < .001$ by Kruskal–Wallis test followed by Dunn's multiple comparison test) as well as that in the SNL contralateral side ($P < .001$ by the Mann–Whitney test). There was no significant difference between other combinations. Finally, we compared the S/N ratio of ATF3+ and ATF3− neurons in the SNL ipsilateral L4 DRG (Fig. 9E–G). We identified 207 N52−/ATF3−, 4 N52−/ATF3+, 217 N52+/ATF3−, and 17 N52+/ATF3+ profiles. Most ATF3+ neuronal profiles had relatively lower signals for BDNF (arrow and arrowhead in Fig. 9E and F). However, there was no significant difference in S/N ratio between N52+/ATF3+ and N52+/ATF3− cells (red and black dots in Fig. 9G, respectively; $P > .5$ by the Mann–Whitney U test). All four N52−/ATF3+ cells were not labeled for BDNF (S/N ratio <6, red dots in Fig. 9G). However, the sample size was too small to reach significance ($P = .12$). In any case, a limited number of injured neurons are not the main contributor to BDNF up-regulation in the L4 DRG after L5 SNL.

4. Discussion

4.1. ATF3+ L4 DRG neurons

ATF3 is a widely used marker for injured DRG neurons following peripheral nerve injury [41]. Shortland et al. [40] and Djouhri et al. [10] demonstrated that 11–40% of L4 DRG nuclei were immuno-

stained for ATF3 after L5 SNL, and proposed that the ipsilateral L4 DRG neurons are not completely spared from injury. We agree with their proposal, as we also observed some ATF3+ nuclei in the L4 DRG (Fig. 2). However, the percentages of ATF3+ nuclei in this study were less than their values (Table 1). These differences are likely to the result of differences in the surgical procedures. As mentioned in Section 2, we paid special attention to avoid the incision of the skin and muscles more rostral than the L5/6 zygapophysial joint. This procedure minimizes the direct injury to the L4 spinal nerve branches (perhaps its dorsal ramus). In fact, accidental skin incision and muscle separation at one level rostral to the aimed lumbar level in a rat induced ATF3 in approximately 34% of the identified nuclei in the ipsilateral L4 DRG (this rat was omitted from this study). This value is similar to those observed in the L5 DRG of sham-operated rats in a previous study [40] and the L4 DRG of SNL rats by another group [10]. In any case, a small population of the L4 DRG neurons could be injured by surgical procedures of L5 SNL (see below). Because the number of neurons that are damaged in the L4 DRG largely depends on the surgical procedures, surgical procedures should be performed carefully to spare the maximum number of L4 DRG neurons, and verification of the proportion of the uninjured L4 DRG neurons is necessary to examine the histochemical changes of the L4 DRG in this neuropathic pain model. A recent study has demonstrated percentages (<3.6%) of ATF3+ neurons in the L4 DRG similar to those in our own results (Table 1) [21].

4.2. Phenotypic changes of ATF3+ neurons in the L4 DRG

Because a small number of L4 DRG neurons were ATF3+ (Figs. 2, 3 and Table 1), the next issue was whether these neurons were accompanied by pain-related phenotypic changes. These neurons may explain the occurrence of spontaneous discharges recorded from the L4 dorsal root in this model [1,4,10,27,31,46]. Expression of both Nav1.3 and NPY are up-regulated by DRG neurons which suffered peripheral axonal injury. Nav1.3 is implicated in the hyperexcitability of these neurons [7,45], and NPY is proposed as an important mediator of mechanical allodynia in this neuropathic pain model [35]. Indeed, we verified clear induction of both NPY and Nav1.3 mRNAs in the directly injured L5 DRG (Figs. 4B and 5B). *De novo* expression of NPY mRNA was also evident in ATF3+ large L4 DRG neurons (Fig. 4C–E). However, we could not detect significant up-regulation of Nav1.3 in the total neuronal population of the ipsilateral L4 DRG (Fig. 5C, F, G). These observations are consistent with previous reports [36,40]. While direct comparison revealed that Nav1.3 S/N ratio of ATF3+ cells was higher than that of ATF3− cells in the SNL ipsilateral L4 DRG (Fig. 5J), the values of ATF3+ cells (S/N ratio ~20) were much less than those of the ipsilateral L5 DRG neurons (Fig. 5E). This phenotypic mismatch between the L4 and L5 ATF3+ neurons may due to the fact that branches of the L4 spinal nerves (perhaps its dorsal ramus) are injured near their peripheral terminals during the back muscle separation during the surgical procedure, whereas the L5 spinal nerve fibers are injured in their mid-axon far from their terminals by ligation. Such a distal axonal injury may be enough to induce ATF3 (Fig. 2) and NPY (Fig. 4) but not to clearly up-regulate Nav1.3 (Fig. 5) in the total neuronal population of the ipsilateral L4 DRG. Thus, although spontaneous discharges in the peripherally injured primary afferents are ascribed to the up-regulation of Nav1.3 in their cell bodies [4,7], carefully performed L5 SNL surgery did not induce Nav1.3 in the L4 DRG, at least to similar high levels as L5 DRG. These data suggest that spontaneous discharges recorded from the L4 dorsal root are the result of some different mechanisms other than changes in Nav1.3 expression, such as inflammatory mediators [5,11,43,47]. With regard to the ATF3+ C-fiber neurons, it is noteworthy that these neurons mostly lacked the nociceptor-specific TTX-r channels, Nav1.8 and Nav1.9, that are proposed as important contributors in some abnormal pain states [2,26], suggesting that these neurons lost some important neurophysiological properties as nociceptors. Anyway, as it is hard to find such a small number of injured L4 fibers during electrophysiological study, the spontaneous discharges should be recorded from the frankly spared L4 fibers.

In conclusion, carefully performed L5 SNL animals and sham-operated animals displayed a quantitatively similar limited number of ATF3 induction in the L4 DRG. However, neuropathic pain behaviors were quite different (Fig. 1). We found that ATF3+ DRG neurons had relatively higher signals for Nav1.3 (Fig. 5J) and significantly lower signals for Nav1.8 and Nav1.9 (Fig. 8C and F) as compared with ATF3− neurons in the SNL ipsilateral L4 DRG. However, the signals for Nav1.3 of the L4 ATF3+ neurons are much less than those of the directly injured L5 DRG neurons (Fig. 5E and F), and the selective loss of Nav1.8 and Nav1.9 signals of the L4 ATF3+ neurons suggests malfunction as nociceptors. Comparison of the total neuronal populations among L4 DRGs from naïve, SNL, and sham-operated rats could not detect significant differences in the expression of all examined Nav mRNAs (Fig. 6). Taking our results all together, it is clear that the small number of injured L4 neurons likely do not contribute to the pathomechanisms of neuropathic pain.

4.3. Phenotypic changes of ATF3− neurons in the L4 DRG

With regard to the changes in expression of Navs in the L4 DRG after L5 SNL, there are controversial studies. Although RT-PCR studies have detected up-regulation of several Navs, especially Nav1.8 mRNA [3,4], immunohistochemical studies have failed [8,25] except for the first study [38]. Because the RT-PCR method cannot reveal which neuronal population contributes to the phenotypic change and the immunohistochemical method cannot detect changes in the protein level in individual cell when there is no change in the number of positively labeled cells, we addressed this issue by comparison of signal intensities (S/N ratio) for Nav mRNAs of individual neurons with smaller ($\leqslant$1000 μm^2, mostly C-fiber neurons) and larger (>1000 μm^2, exclusively A-fiber neurons) cell bodies using ISHH (Fig. 6). However, we could not detect any significant changes in the expression of all examined Nav mRNAs in the SNL ipsilateral L4 DRG. Indeed, ISHH may not be a strictly quantitative method as is RT-PCR, but our method is highly sensitive for expressional changes in a limited number of neurons (Fig. 5J). In any case, the up-regulation of Nav1.8 mRNA in the SNL ipsilateral L4 DRG needs further study. It may be noteworthy that A-fiber neurons tend to slightly increase this channel in the L4 DRG, although it did not reach statistical significance (Fig. 6L).

BDNF is one of the most important pain neuromodulators at the synapses between the primary afferents and the spinal dorsal horn neurons [28,37]. Although the expression of BDNF is up-regulated in both the directly injured and the spared DRGs, this change occurs in neurochemically different neuronal populations. In the spared DRG, BDNF increases almost exclusively in TrkA-expressing cells [13]. On the other hand, in the injured DRG, BDNF increases in TrkB or TrkC-expressing medium to large neurons, but not in TrkA-expressing neurons [29]. Because TrkA is expressed by both C-fiber and A-fiber neurons [14], we analyzed BDNF expression separately in C-fiber and A-fiber populations (Fig. 9). Our results indicate that the ATF3+ neurons are not the main contributor to BDNF up-regulation in the L4 DRG (red dots in Fig. 9G). Thus, we show that some uninjured DRG neurons maintaining anatomical connection with the peripheral receptive field increased BDNF. This is also the case after chronic constriction injury of the sciatic nerve in rats [33]. We again propose that the clearly spared L4 DRG neurons increase this neuromodulator and contribute to sensory hypersensitivity induced by L5 SNL [13].

Conflicts of interest statement

The authors declare no financial or other conflicts of interest related to this study.

Acknowledgement

This work was supported by Grant-in Aid (Grant No. 19603019) from the Japanese Ministry of Education, Science and Culture.

References

[1] Ali Z, Ringkamp M, Hartke TV, Chien HF, Flavahan NA, Campbell JN, Meyer RA. Uninjured C-fiber nociceptors develop spontaneous activity and alpha-adrenergic sensitivity following L6 spinal nerve ligation in monkey. J Neurophysiol 1999;81:455–66.
[2] Amaya F, Wang H, Costigan M, Allchorne AJ, Hatcher JP, Egerton J, Stean T, Morisset V, Grose D, Gunthorpe MJ, Chessell IP, Tate S, Green PJ, Woolf CJ. The voltage-gated sodium channel Na(v)1.9 is an effector of peripheral inflammatory pain hypersensitivity. J Neurosci 2006;26:12852–60.
[3] Berta T, Poirot O, Pertin M, Ji RR, Kellenberger S, Decosterd I. Transcriptional and functional profiles of voltage-gated Na(+) channels in injured and non-injured DRG neurons in the SNI model of neuropathic pain. Mol Cell Neurosci 2008;37:196–208.
[4] Boucher TJ, Okuse K, Bennett DL, Munson JB, Wood JN, McMahon SB. Potent analgesic effects of GDNF in neuropathic pain states. Science 2000;290:124–7.
[5] Bove GM, Ransil BJ, Lin HC, Leem JG. Inflammation induces ectopic mechanical sensitivity in axons of nociceptors innervating deep tissues. J Neurophysiol 2003;90:1949–55.
[6] Cho HJ, Kim JK, Park HC, Kim JK, Kim DS, Ha SO, Hong HS. Changes in brain-derived neurotrophic factor immunoreactivity in rat dorsal root ganglia, spinal cord, and gracile nuclei following cut or crush injuries. Exp Neurol 1998;154:224–30.
[7] Chung JM, Chung K. Sodium channels and neuropathic pain. Novartis Found Symp 2004;261:19–27. discussion 31, 47–54.
[8] Decosterd I, Ji RR, Abdi S, Tate S, Woolf CJ. The pattern of expression of the voltage-gated sodium channels Na(v)1.8 and Na(v)1.9 does not change in uninjured primary sensory neurons in experimental neuropathic pain models. Pain 2002;96:269–77.
[9] Devor M. Ectopic discharge in Abeta afferents as a source of neuropathic pain. Exp Brain Res 2009;196:115–28.
[10] Djouhri L, Koutsikou S, Fang X, McMullan S, Lawson SN. Spontaneous pain, both neuropathic and inflammatory, is related to frequency of spontaneous firing in intact C-fiber nociceptors. J Neurosci 2006;26:1281–92.
[11] Eliav E, Benoliel R, Tal M. Inflammation with no axonal damage of the rat saphenous nerve trunk induces ectopic discharge and mechanosensitivity in myelinated axons. Neurosci Lett 2001;311:49–52.
[12] Fukuoka T, Kobayashi K, Yamanaka H, Obata K, Dai Y, Noguchi K. Comparative study of the distribution of the alpha-subunits of voltage-gated sodium channels in normal and axotomized rat dorsal root ganglion neurons. J Comp Neurol 2008;510:188–206.
[13] Fukuoka T, Kondo E, Dai Y, Hashimoto N, Noguchi K. Brain-derived neurotrophic factor increases in the uninjured dorsal root ganglion neurons in selective spinal nerve ligation model. J Neurosci 2001;21:4891–900.
[14] Fukuoka T, Noguchi K. Comparative study of voltage-gated sodium channel α-subunits in non-overlapping four neuronal populations in the rat dorsal root ganglion. Neurosci Res 2011;70:164–71.
[15] Fukuoka T, Noguchi K. Contribution of the spared primary afferent neurons to the pathomechanisms of neuropathic pain. Mol Neurobiol 2002;26:57–67.
[16] Fukuoka T, Tokunaga A, Kondo E, Miki K, Tachibana T, Noguchi K. Change in mRNAs for neuropeptides and the GABA(A) receptor in dorsal root ganglion neurons in a rat experimental neuropathic pain model. Pain 1998;78:13–26.
[17] Fukuoka T, Tokunaga A, Tachibana T, Dai Y, Yamanaka H, Noguchi K. VR1, but not P2X(3), increases in the spared L4 DRG in rats with L5 spinal nerve ligation. Pain 2002;99:111–20.
[18] Goldin AL, Barchi RL, Caldwell JH, Hofmann F, Howe JR, Hunter JC, Kallen RG, Mandel G, Meisler MH, Netter YB, Noda M, Tamkun MM, Waxman SG, Wood JN, Catterall WA. Nomenclature of voltage-gated sodium channels. Neuron 2000;28:365–8.
[19] Ha SO, Kim JK, Hong HS, Kim DS, Cho HJ. Expression of brain-derived neurotrophic factor in rat dorsal root ganglia, spinal cord and gracile nuclei in experimental models of neuropathic pain. Neuroscience 2001;107:301–9.
[20] Hudson LJ, Bevan S, Wotherspoon G, Gentry C, Fox A, Winter J. VR1 protein expression increases in undamaged DRG neurons after partial nerve injury. Eur J Neurosci 2001;13:2105–14.
[21] Jeon SM, Lee KM, Cho HJ. Expression of monocyte chemoattractant protein-1 in rat dorsal root ganglia and spinal cord in experimental models of neuropathic pain. Brain Res 2009;1251:103–11.
[22] Katsura H, Obata K, Mizushima T, Yamanaka H, Kobayashi K, Dai Y, Fukuoka T, Tokunaga A, Sakagami M, Noguchi K. Antisense knock down of TRPA1, but not TRPM8, alleviates cold hyperalgesia after spinal nerve ligation in rats. Exp Neurol 2006;200:112–23.
[23] Kim SH, Chung JM. An experimental model for peripheral neuropathy produced by segmental spinal nerve ligation in the rat. Pain 1992;50:355–63.
[24] Kobayashi K, Fukuoka T, Yamanaka H, Dai Y, Obata K, Tokunaga A, Noguchi K. Neurons and glial cells differentially express P2Y receptor mRNAs in the rat dorsal root ganglion and spinal cord. J Comp Neurol 2006;498:443–54.
[25] Lai J, Gold MS, Kim CS, Bian D, Ossipov MH, Hunter JC, Porreca F. Inhibition of neuropathic pain by decreased expression of the tetrodotoxin-resistant sodium channel, NaV1.8. Pain 2002;95:143–52.
[26] Lai J, Porreca F, Hunter JC, Gold MS. Voltage-gated sodium channels and hyperalgesia. Annu Rev Pharmacol Toxicol 2004;44:371–97.
[27] Ma C, Shu Y, Zheng Z, Chen Y, Yao H, Greenquist KW, White FA, LaMotte RH. Similar electrophysiological changes in axotomized and neighboring intact dorsal root ganglion neurons. J Neurophysiol 2003;89:1588–602.
[28] Merighi A, Salio C, Ghirri A, Lossi L, Ferrini F, Betelli C, Bardoni R. BDNF as a pain modulator. Prog Neurobiol 2008;85:297–317.
[29] Michael GJ, Averill S, Shortland PJ, Yan Q, Priestley JV. Axotomy results in major changes in BDNF expression by dorsal root ganglion cells: BDNF expression in large trkB and trkC cells, in pericellular baskets, and in projections to deep dorsal horn and dorsal column nuclei. Eur J Neurosci 1999;11:3539–51.
[30] Miki K, Fukuoka T, Tokunaga A, Noguchi K. Calcitonin gene-related peptide increase in the rat spinal dorsal horn and dorsal column nucleus following peripheral nerve injury: up-regulation in a subpopulation of primary afferent sensory neurons. Neuroscience 1998;82:1243–52.
[31] Nassar MA, Baker MD, Levato A, Ingram R, Mallucci G, McMahon SB, Wood JN. Nerve injury induces robust allodynia and ectopic discharges in Nav1.3 null mutant mice. Mol Pain 2006;2:33.
[32] Noguchi K, Kawai Y, Fukuoka T, Senba E, Miki K. Substance P induced by peripheral nerve injury in primary afferent sensory neurons and its effect on dorsal column nucleus neurons. J Neurosci 1995;15:7633–43.
[33] Obata K, Yamanaka H, Fukuoka T, Yi D, Tokunaga A, Hashimoto N, Yoshikawa H, Noguchi K. Contribution of injured and uninjured dorsal root ganglion neurons to pain behavior and the changes in gene expression following chronic constriction injury of the sciatic nerve in rats. Pain 2003;101:65–77.
[34] Obata K, Yamanaka H, Kobayashi K, Dai Y, Mizushima T, Katsura H, Fukuoka T, Tokunaga A, Noguchi K. Role of mitogen-activated protein kinase activation in injured and intact primary afferent neurons for mechanical and heat hypersensitivity after spinal nerve ligation. J Neurosci 2004;24:10211–22.
[35] Ossipov MH, Zhang ET, Carvajal C, Gardell L, Quirion R, Dumont Y, Lai J, Porreca F. Selective mediation of nerve injury-induced tactile hypersensitivity by neuropeptide Y. J Neurosci 2002;22:9858–67.
[36] Pertin M, Ji RR, Berta T, Powell AJ, Karchewski L, Tate SN, Isom LL, Woolf CJ, Gilliard N, Spahn DR, Decosterd I. Upregulation of the voltage-gated sodium channel beta2 subunit in neuropathic pain models: characterization of expression in injured and non-injured primary sensory neurons. J Neurosci 2005;25:10970–80.
[37] Pezet S, McMahon SB. Neurotrophins: mediators and modulators of pain. Annu Rev Neurosci 2006;29:507–38.
[38] Porreca F, Lai J, Bian D, Wegert S, Ossipov MH, Eglen RM, Kassotakis L, Novakovic S, Rabert DK, Sangameswaran L, Hunter JC. A comparison of the potential role of the tetrodotoxin-insensitive sodium channels, PN3/SNS and NaN/SNS2, in rat models of chronic pain. Proc Natl Acad Sci USA 1999;96:7640–4.
[39] Potrebic S, Ahn AH, Skinner K, Fields HL, Basbaum AI. Peptidergic nociceptors of both trigeminal and dorsal root ganglia express serotonin 1D receptors: implications for the selective antimigraine action of triptans. J Neurosci 2003;23:10988–97.
[40] Shortland PJ, Baytug B, Krzyzanowska A, McMahon SB, Priestley JV, Averill S. ATF3 expression in L4 dorsal root ganglion neurons after L5 spinal nerve transection. Eur J Neurosci 2006;23:365–73.
[41] Tsujino H, Kondo E, Fukuoka T, Dai Y, Tokunaga A, Miki K, Yonenobu K, Ochi T, Noguchi K. Activating transcription factor 3 (ATF3) induction by axotomy in sensory and motoneurons: a novel neuronal marker of nerve injury. Mol Cell Neurosci 2000;15:170–82.
[42] Vellani V, Colucci M, Lattanzi R, Giannini E, Negri L, Melchiorri P, McNaughton PA. Sensitization of transient receptor potential vanilloid 1 by the prokineticin receptor agonist Bv8. J Neurosci 2006;26:5109–16.
[43] Wang JG, Strong JA, Xie W, Yang RH, Coyle DE, Wick DM, Dorsey ED, Zhang JM. The chemokine CXCL1/growth related oncogene increases sodium currents and neuronal excitability in small diameter sensory neurons. Mol Pain 2008;4:38.
[44] Wang R, Guo W, Ossipov MH, Vanderah TW, Porreca F, Lai J. Glial cell line-derived neurotrophic factor normalizes neurochemical changes in injured dorsal root ganglion neurons and prevents the expression of experimental neuropathic pain. Neuroscience 2003;121:815–24.
[45] Waxman SG, Dib-Hajj S, Cummins TR, Black JA. Sodium channels and pain. Proc Natl Acad Sci USA 1999;96:7635–769.
[46] Wu G, Ringkamp M, Hartke TV, Murinson BB, Campbell JN, Griffin JW, Meyer RA. Early onset of spontaneous activity in uninjured C-fiber nociceptors after injury to neighboring nerve fibers. J Neurosci 2001;21:RC140 (1–5).
[47] Wu G, Ringkamp M, Murinson BB, Pogatzki EM, Hartke TV, Weerahandi HM, Campbell JN, Griffin JW, Meyer RA. Degeneration of myelinated efferent fibers induces spontaneous activity in uninjured C-fiber afferents. J Neurosci 2002;22:7746–53.
[48] Zimmermann M. Ethical guidelines for investigations of experimental pain in conscious animals. Pain 1983;16:109–10.

Yoshida et al. Molecular Pain 2011, 7:41
http://www.molecularpain.com/content/7/1/41

MOLECULAR PAIN

RESEARCH Open Access

Inhibition of TRPA1 channel activity in sensory neurons by the glial cell line-derived neurotrophic factor family member, artemin

Naoki Yoshida[1,2], Kimiko Kobayashi[1,2], Lina Yu[1,2], Shenglan Wang[1,2], Rengaowa Na[1,3], Satoshi Yamamoto[1], Koichi Noguchi[2] and Yi Dai[1,2*]

Abstract

Background: The transient receptor potential (TRP) channel subtype A1 (TRPA1) is known to be expressed on sensory neurons and respond to changes in temperature, pH and local application of certain noxious chemicals such as allyl isothiocyanate (AITC). Artemin is a neuronal survival and differentiation factor and belongs to the glial cell line-derived neurotrophic factor (GDNF) family. Both TRPA1 and artemin have been reported to be involved in pathological pain initiation and maintenance. In the present study, using whole-cell patch clamp recording technique, *in situ* hybridization and behavioral analyses, we examined the functional interaction between TRPA1 and artemin.

Results: We found that 85.8 ± 1.9% of TRPA1-expressing neurons also expressed GDNF family receptor alpha 3 (GFR α3), and 87.5 ± 4.1% of GFRα3-expressing neurons were TRPA1-positive. In whole-cell patch clamp analysis, a short-term treatment of 100 ng/ml artemin significantly suppressed the AITC-induced TRPA1 currents. A concentration-response curve of AITC resulting from the effect of artemin showed that this inhibition did not change EC_{50} but did lower the AITC-induced maximum response. In addition, pre-treatment of artemin significantly suppressed the number of paw lifts induced by intraplantar injection of AITC, as well as the formalin-induced pain behaviors.

Conclusions: These findings that a short-term application of artemin inhibits the TRPA1 channel's activity and the sequential pain behaviors suggest a role of artemin in regulation of sensory neurons.

Background

Artemin belongs to glial cell line-derived neurotrophic factor (GDNF) family that regulates the development and the function of the nervous system. Artemin binds to the GFR α3/RET receptor complex and then activates several intracellular signaling pathways [1]. Artemin supports survival of sensory neurons *in vitro* and *in vivo* apparently by interacting with GFRα3, which is highly restricted in adult to neurons of the peripheral nervous system (sensory and sympathetic). GFRα3 is expressed by a subpopulation of nociceptive sensory neurons, some or all of which also express the Ret receptor tyrosine kinase, the transient receptor potential (TRP) ion channel proteins TRPV1 and TRPA1 [2,3]. The expression of these channels in GFR α3-positive neurons suggests that artemin signaling *via* GFR α3/Ret binding could modulate neuron sensitivity.

TRPA1 is a member of branch A of the TRP family of cation channels[4] and is expressed by a subset of small-sized DRG or trigeminal ganglia neurons in neonatal rats, adult rats and mice [5-7]. TRPA1 has been reported to be activated by various kinds of noxious compounds through covalent modification of cysteines [5,8-13]. TRPA1 is also activated by an endogenous aldehyde, 4-hydroxynonenal, bradykinin, intracellular pH and CO2 [8,14-16]. Studies using knockout mice demonstrated that TRPA1 is an important component of the transduction machinery through which environmental irritants and endogenous proalgesic agents depolarize nociceptors to elicit inflammatory pain [17,18]. A

* Correspondence: ydai@huhs.ac.jp
[1]Department of Pharmacy, School of Pharmacy, Hyogo University of Health Sciences, Kobe, Hyogo 650-8530, Japan
Full list of author information is available at the end of the article

recent report showing the nearly complete attenuation of formalin-induced pain behaviors by pharmacological blockade or genetic ablation indicated that TRPA1 is crucial in inflammatory pain [19]. Taking the above into account, it is clear that this channel is importantly involved in pain transmission in the primary afferents and a potential target for analgesic development.

Recent reports suggested that artemin potentiates TRPV1 signaling and induces behavioral hyperalgesia. Overexpression of artemin increased the expression and sensitivity of TRPV1 and TRPA1 in trigeminal afferents signaling and induced behavioral hyperalgesia [20,21]. We have studied the modulation mechanism of TRPV1 and TRPA1 by inflammatory modulators and reported that trypsin/tryptase-PAR2 signaling or bradykinin-B2R signaling sensitizes TRPA1 channel through PLC and/or PKA pathways to induce inflammatory pain [22-24]. In the present study, we hypothesized that a functional interaction of artemin and TRPA1 might contribute to the pathogenesis of inflammatory pain. We observed high co-expression of the TRPA1 with the GFR α3 receptor and found a significant enhancement of desensitization of TRPA1 activity induced by artemin in rat DRG neurons, which was also confirmed at the behavioral level.

Methods

Immunohistochemistry

All animal experimental procedures were approved by the Hyogo University of Health Sciences Committee on Animal Research (#2008-05, #2008-10) and were performed in accordance with the National Institutes of Health guidelines on animal care. Adult male Sprague-Dawley (SD) rats (220-250 g; Japan Animals, Osaka, Japan) were perfused transcardially with 1% paraformaldehyde in 0.1 M phosphate buffer followed by 4% paraformaldehyde in 0.1 M phosphate buffer (PB, pH 7.4). The L4-5 DRGs were removed and processed for TRPA1 immunohistochemistry as described in our previous study [23]. For double immunofluorescence, tyramide signal amplification (TSA; NEN) fluorescence procedures were used for TRPA1 (1:10,000) staining. The raised rabbit primary antibody for TRPA1 [23] and biotin conjugated Griffonia simplicifolia Isolectin B4 (IB4, Sigma, St. Louis, MO) at 1:1000 combined with Alexa fluor 488 goat anti-rabbit IgG (1:500; Invitrogen/Molecular Probes, Inc., Carlsbad, CA) and strept-avidin conjugated with Alexa fluor 594 (1:500: Invitrogen/Molecular Probes), respectively, were used for double immunofluorescence staining [22].

In situ hybridization histochemistry (ISHH)

Adult male SD rats weighing 200-250 g were killed by decapitation under deep ether anesthesia. The bilateral L4, L5 DRGs were dissected out, rapidly frozen in powdered dry ice, and cut on a cryostat at a 5 μm thickness. Sections were thaw mounted onto MAS-coated glass slides (Matsunami, Osaka, Japan) and fixed in 4% formaldehyde in 0.1 M PB (pH 7.4) for 20 min. After washing with PB, the sections were treated with 10 μg/ml protease K in 50 mM Tris/5 mM EDTA (pH 8.0) for 3 min at room temperature, postfixed in the same fixative, acetylated with acetic anhydride in 0.1 M triethanolamine, rinsed with PB, and dehydrated through an ascending ethanol series. For dual ISHH of TRPA1 and GDNF family receptors, we used a DIG-labeled probe for TRPA1 (GenBank accession number AY496961, nucleotides 302 - 769) and a ^{35}S-labeled RNA probe for Ret (GenBank accession number U22513, nucleotides 13-319), GFR α1 (GenBank accession number U97142, nucleotides 652 - 955), or GFR α2 (GenBank accession number U97143, nucleotides 362 - 702), or GFR α3 (GenBank accession number AF184920, nucleotides 164 - 604) in the same sections, respectively. The details of the dual ISHH procedure have been described in our previous study [6].

Mammalian cell culture

For primary culture of DRG neurons, DRGs were collected from the adult SD rats (100-200 g) using sterile techniques, and placed in ice-cold Earle's balanced salt solution (EBSS, Sigma). Adhering fat and connective tissue were removed and each DRG was placed immediately in a medium consisting of 2 ml of EBSS and 1.25 mg/ml of collagenase P (Sigma) and kept at 37°C for 60 min with occasional agitation. After dissociation of the DRG cells, this cell suspension was centrifuged for 5 min at 1000 rpm and the cell pellet was re-suspended in EBSS supplemented with 10% fetal bovine serum (FBS), 2 mM glutamax, penicillin, streptomycin and vitamin solution. Recombinant rat nerve growth factor (100 ng/ml, Sigma) was added to the medium.

Electrophysiology

Whole-cell patch-clamp recordings were carried out at 1 day after dissociation of the DRG neurons. Voltage-clamp experiments were performed at -60 mV holding potential, and recordings were sampled at 5 kHz and filtered at 2 kHz. Current densities (pA/pF) and normalized currents (the third currents were normalized to the second currents evoked by an agonist) were measured. The current magnitude was quantified by peak current amplitude in all experiments. A normalized current was obtained by normalizing the third application-induced current to the second one, and just in case the magnitude of the second current by agonist was larger than a half of the first current to

evaluate the results under less effect of the desensitization by the first current. In experiments with DRG neurons, after AITC (300 μM) application, capsaicin (10 μM) was applied at the end of recording to identify whether the AITC-induced current was mediated by TRPA1 channels. Data were obtained just in case the DRG neuron was sensitive to both AITC and capsaicin application, since an AITC-activated current in capsaicin-sensitive DRG neurons is certainly a TRPA1-mediated event [18]. The standard bath solution contained 140 mM NaCl, 5 mM KCl, 2 mM $MgCl_2$, 2 mM $CaCl_2$, 10 mM HEPES and 10 mM glucose, pH 7.4 (adjusted with NaOH). In some experiments, artemin (100 ng/ml) was included in the bath solutions. The pipette solution contained 140 mM KCl, 2 mM $MgCl_2$, 0.5 mM $CaCl_2$, 5 mM MgATP, 5 mM EGTA and 5 mM HEPES, pH 7.2 (adjusted with Tris-base). The concentration-response curves for the effect of artemin on AITC-induced current densities (pA/pF) were fit by the Hill equation using Origin 8.1 (OriginLab Corporation, Northampton, MA, USA). All patch-clamp experiments were performed at room temperature (~25°C; RT). The solutions containing drugs were applied to the chamber (180 μl) by a gravity system at a flow rate of 4-7 ml/min.

Behavioral studies

Sixteen and 10 male adult SD rats (200-250 g) were used for the AITC-induced nocifensive behavioral analyses and formalin test, respectively. After adaptation, 50 μl artemin (10 μg/ml, in PBS) or PBS was injected intraplantarly into the rat left hind paw. Five minutes after these injections, rats received intradermal injection of 50 μl of AITC (3% in liquid paraffin, Wako Pure Chemical Industries, Ltd., Osaka, Japan) or formalin (3% in saline) to the same area of artemin-injected plantar surface. The rats were placed in a wire mesh cage immediately after the injection. The numbers of hind paw lifts and durations of flinches per 5 min interval during the initial 30 min post-injection of AITC and 60 min post-infection of formalin period were measured for the AITC-induced nocifensive behavior and formalin test, respectively. The total number of lifts and durations of flinches during the entire initial 30 min for AITC and 60 min for formalin post-injection were also calculated.

Statistical analysis

All results are expressed as mean ± SEM. An unpaired t-test or ANOVA followed by Fisher's PLSD was used to compare the calcium imaging data and electrophysiological data between the groups. Two-way repeated ANOVA followed by Fisher's PLSD was applied to the behavioral data. A difference was accepted as significant if the probability was less than 5% ($p < 0.05$).

Results

Colocalization of TRPA1 with GDNF family receptors in rat DRG neurons

Nociceptors can be neurochemically classified into two subpopulations and modulated by neurotrophic factors differently in each population. Double immunofluorescent staining indicated that 82.2 ± 1.1% of TRPA1 positive neurons were also labeled with IB4, a marker of the nonpeptidergic and GDNF family members-dependent neurons, and 44.1 ± 1.9% of IB4-positive neurons were also stained for TRPA1 (Figure 1A). To further determine the histological evidence of colocalization with TRPA1 and GDNF family receptors, we examined the co-localization of TRPA1 mRNAs with Ret, GFR α1, GFR α2, and GFR α3 mRNAs using double ISHH (Figure 1B-E). We observed these mRNAs were expressed in 36.9 ± 2.6% (TRPA1), 77.4 ± 3.2% (Ret), 45.6 ± 4.9% (GFR α1), 44.1 ± 1.7% (GFR α2) and 38.4 ± 2.7% (GFR α3) of the total neuronal profiles. A significant population of TRPA1-positive neurons were also labeled for c-Ret and GFR α3 (arrows in Figure 1B, E) in the DRG (Table 1). The high percentages of colocalization: 99.3 ± 0.6% and 85.8 ± 1.9% of TRPA1 expressing neurons were Ret- and GFR α3-positive, respectively, suggest that TRPA1 is selectively expressed by artemin-sensitive Ret/GFR α3 neurons (Figure 1B and 1E). In contrast to the high incidence of co-localization of TRPA1 and GFR α3, only 13.5 ± 7.7% and 45.9 ± 7.6% of TRPA1-positive neurons were also labeled for GFR α1 and GFR α2, respectively (Figure 1C and 1D). This high percentage of co-expression of TRPA1 with GFR α3 in DRG neurons indicates a possible interaction between them in primary afferent neurons.

Artemin suppresses AITC-induced current in DRG neurons

Based on the histological results, we hypothesized that artemin may play important roles in the functional modulation of TRPA1. To this end, we performed whole-cell voltage-clamp experiments in cultured rat DRG neurons. We found that application of artemin alone to cause no change of membrane currents in cultured DRG neurons. AITC, as a selective activator of TRPA1, had been used in patch-clamp experiment to detect the TRPA1 current. A previous study indicates that there are still AITC-sensitive cells in TRPA1 knockout mice, but these are not the TRPV1-expressing cells where most TRPA1 is expressed [18]. To confirm the AITC-evoked current in DRG is a TRPA1-mediated event, capsaicin at 10 μM was applied at the end of recording using the patch-clamp preparation (see Materials and Methods section).

We observed that the AITC-activated inward currents in DRG neurons underwent a weak tachphylaxis, giving a smaller response on repeated applications of 300 μM

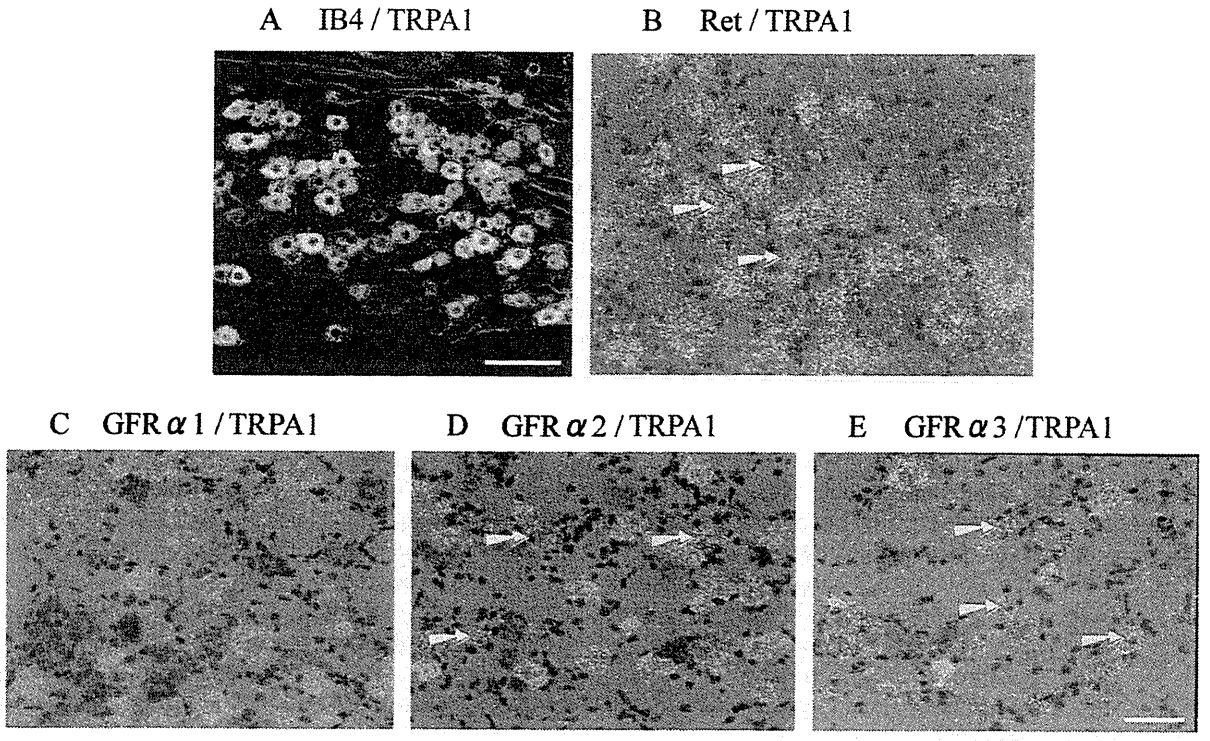

Figure 1 Colocalization of TRPA1 and IB4, Ret or GFR αs in DRG neurons. (A): Double immunostaining of TRPA1 (green) and IB4 (red) showed almost all of TRPA1 were expressed in IB4-labeled neurons of the naïve rat DRG. (B-E): Colocalization of TRPA1 mRNA (brown cells) and Ret (B), GFR α1 (C), GFR α2 (D), and GFR α3 (E) mRNAs (clusters of silver grains) using double ISHH with ^{35}S-labeled antisense Ret and GFR αs probes combined with TRPA1 DIG-labeled probe. The bright field and dark field photographs are merged. Arrows indicate examples of double-labeled neurons. Scale bar = 100 μm in A, = 50 μm in B-D.

AITC for 20 sec (Figure 2A). We have previously demonstrated that G protein-coupled receptor signals can potentiate the TRPA1 activity [23,24]. However, in the present study, instead of potentiation, after 2 min pretreatment with artemin (100 ng/ml), reapplication of AITC with the same dose produced much smaller current responses than the preceding application of AITC. The normalized currents were significantly smaller in the artemin-pretreated group than that in the control group, which was not pretreated with artemin (0.9 ± 0.09-fold change, n = 11 for control; 0.3 ± 0.09-fold change, n = 6 for artemin; $p < 0.005$). A smaller effect was detected in cells pretreated with artemin in low concentrations (1 ng/ml) (0.8 ± 0.05-fold change, n = 4 for 1 ng/ml $p > 0.05$ versus control) (Figure 2B and 2C). This suppression effect lasted at least 8 min after artemin application (Figure 2D). To further confirm the inhibitory effect of TRPA1 by artemin, we also tested the effect of artemin on AITC-induced current density in DRG neurons. After 2 min pretreatment of artemin, the current density induced by AITC (300 μM, 1 min) was significantly suppressed (-30.8 ± 8.74 pA/pF, n = 8 for control, -9.5 ± 4.25 pA/pF, n = 8 for artemin, $p < 0.05$ vs control) (Figure 3A-C). To examine how artemin changes TRPA1 responsiveness, we measured AITC-induced current density by applying a range of concentrations of AITC in the absence or presence of artemin. We found that treatment of artemin suppressed the maximum response (-64.4 ± 13.36 pA/pF for control vs -19.8 ± 11.16 pA/pF for artemin) without conspicuously affecting EC_{50} (343 μM for control vs 396 μM for artemin) (Figure 3D). These data clearly indicate a suppressive effect of artemin on TRPA1 channel activity.

Table 1 The percentage of DRG profiles that co-express IB4, Ret, GFR α1, GFR α2, or GFR α3 and TRPA1 mRNA (mean ± SE)

x	x/total	TRPA1/x	x/TRPA1
TRPA1	36.9 ± 2.6%	100%	100%
IB4	N.A.	44.1 ± 1.9%	82.2 ± 1.1%
GFR α1	45.6 ± 4.9%	10.2 ± 5.1%	13.5 ± 7.7%
GFR α2	44.1 ± 1.7%	37.8 ± 7.0%	45.9 ± 7.6%
GFR α3	38.4 ± 2.7%	87.5 ± 4.1%	85.8 ± 1.9%
Ret	77.4 ± 3.2%	47.5 ± 5.5%	99.3 ± 0.6%

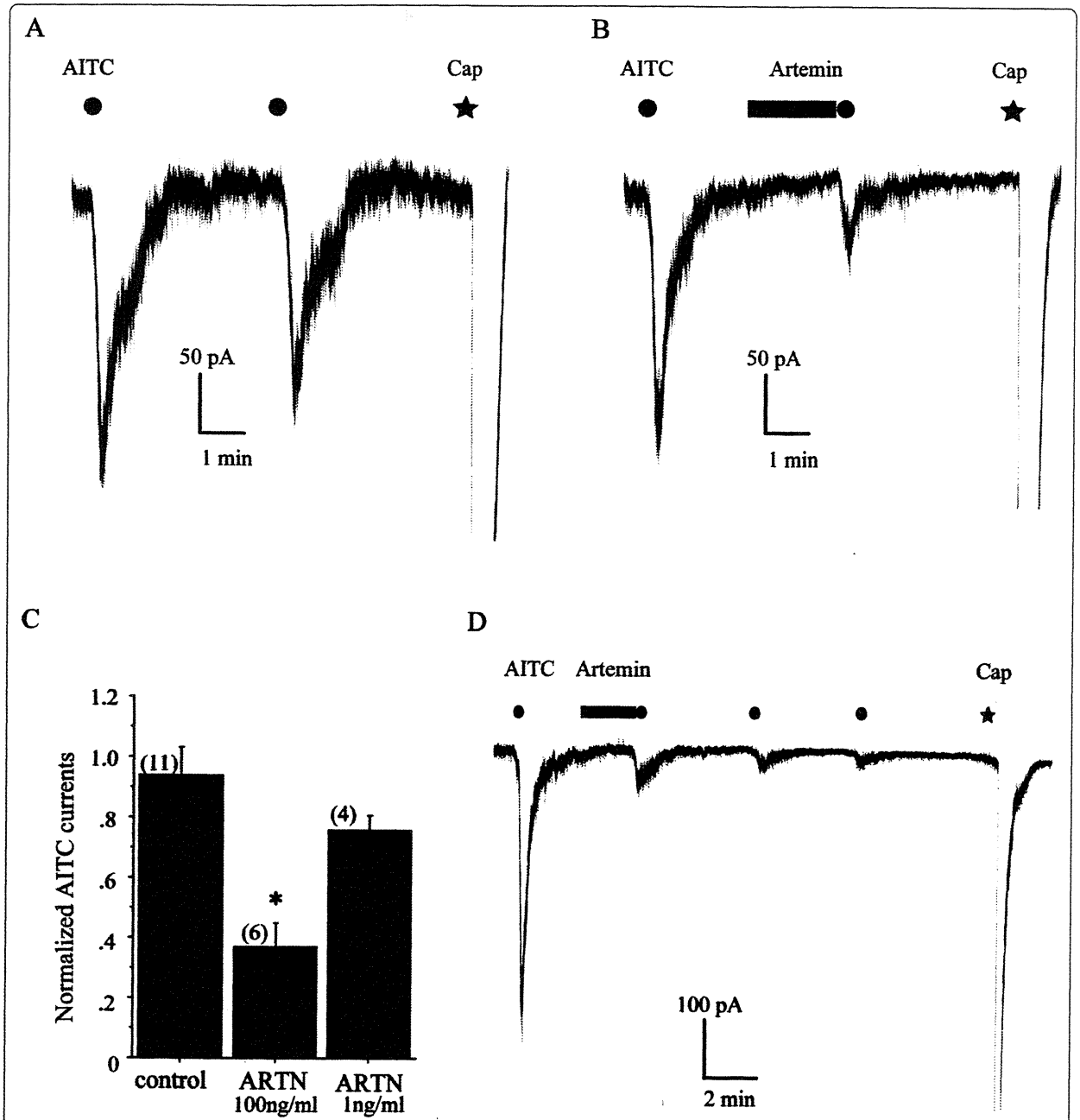

Figure 2 A short-term treatment of artemin decreased AITC-induced currents in DRG neurons. (A, B): Representative traces show TRPA1 currents produced by repeated AITC application without (A) or with (B) artemin (100 ng/ml) treatment. AITC was re-applied after artemin administration for 2 min. (C): Bar graph shows the effect of artemin on AITC activated currents. Currents were normalized to the values evoked initially by AITC application in the absence of artemin. Numbers in parenthesis indicate cells tested. (D): Representative traces show time-course of TRPA1 currents induced by repeated AITC application after artemin (100 ng/ml) treatment. AITC (300 μM) in a bath solution was perfused for 20s in all experiments.

Artemin suppressed TRPA1-mediated pain behaviors

Activation of TRPA1 by pungent natural products suggests a nociceptive role for TRPA1. Both AITC and formalin has been reported to cause nocifensive behaviors in animals through TRPA1 activation [19,23]. To test whether artemin treatment could suppress TRPA1-mediated pain behaviors, we performed intraplantar injections with AITC or formalin after pretreatment of artemin (10 μg/ml) and recorded nocifensive behaviors of rats. Consistent with our previous studies [23-25], both AITC- and formalin-injection